Studies on Novel Antibody for Antibody Therapeutics against Cancer Specific Target, Nectin-2

A Dissertation Submitted to
the Graduate School of Life and Environmental Sciences,
the University of Tsukuba
in Partial Fulfillment of the Requirements
for the Degree of Doctor of Philosophy in Biological Science
(Doctoral Program in Biological Sciences)

Tsutomu OSHIMA

Table of Contents

Abstract

Cancer incidence is one of the most rapidly growing disease worldwide. Current standard of care is mainly small molecule treatment. Cancer cells are rapidly growing compared to normal cells, therefore, those small molecules target mainly growing cells. However, normal cells like skin, colon, bone marrow and hair, also grow very rapidly, and the anti-cancer drugs also affect those first growing normal cells resulted in inducing severe side-effect. Recently, target therapy (or molecular targeted therapy) using antibodies, proteins, or small molecules, are actively researched and developed in many pharmaceuticals. Mainly antibody therapeutics are commonly developed as anti-cancer therapeutics. The main functions of antibodies in body are to neutralize pathogens such as pathogenic bacteria and viruses with high specificity and binding activity. Antibody therapeutics in especially cancer treatment has a potential to inhibit cancer cell growth and/or kill cancer cells with limited side-effect due to the high specificity and binding activity. Antibody therapeutics are multi-function therapeutics depending on the target, its binding site and effector functions. Those functions include cancer cell growth inhibition, induction of apoptosis, CDC, ADCC, ADCP.

To discover novel antibody therapeutics for cancer treatment, I performed gene expression profile analysis, immunohistochemistry and flow cytometry analysis, and discovered in the study described in Chapter 1 that both gene and protein expression level of Nectin-2 were up-regulated in breast and ovarian cancer tissues. I also characterized antibodies in *in vitro* cancer cell growth inhibition, Nectin-2-Nectin-2 or Nectin-2-Nectin-3 *trans* binding inhibition, ADCC, and epitope binning study. Representative antibodies in epitope bin were applied in *in vivo* anti-tumor models. The antibodies showed strong anti-tumor effects in mouse therapeutic models, and I found that its main mechanism of action appeared to be ADCC by performing further *in vivo* studies with IgG_4 forms of

anti-Nectin-2, which did not have ADCC. I performed monkey toxicological study with lead anti-Nectin-2 antibody, Y-443, which is described in Chapter 2. The Y-443, unexpectedly, induced strong platelet reduction, bleeding tendency, hemorrhage in organs, and splenomegaly upon administration, which was similar to symptoms of thrombocytopenia, presumably Y-443 bound to the Nectin-2 on platelet followed by phagocytosis by macrophages, and platelets were digested in spleen. To mitigate this adverse effect, I mutated the Fc region of Y-443 to reduce the Fc binding to Fcγ receptor I, which is the main receptor for phagocytosis on macrophages. In addition, I engineered the Fc through defucosylation to maintain ADCC. The Fc engineered antibody, Y-634, demonstrated diminished thrombocytopenia symptoms with maintaining anti-tumor activity through ADCC in mouse xenograft models. These results from my studies indicate the potential usage of anti-Nectin-2 antibody for the treatment of cancer patients and the potential mitigation strategy by Fc engineering to ameliorate safety liabilities in antibody induced thrombocytopenia.

Abbreviations

ADCC	Antibody-dependent cellular cytotoxicity
APTT	Activated partial thromboplastin time
Asn	Asparagine
Asp	Aspartic acid
ATCC	American Type Culture Collection
BiTE	Bispecific T cell engagers
CDC	Complement-dependent cytotoxicity
CDR	Complementarity determining region
Cyno	Cynomolgus monkey (*Macaca fascicularis*)
D	Aspartic acid
D-PBS	Dulbecco's phosphate-buffered saline
ED	Extracellular domain
ELISA	Enzyme-linked immunosorbent assay
FBS	Fetal bovine serum
FcγR	Fc gamma receptor
FCM	Flow cytometry
HPACC	Health Protection Agency Culture Collections
Ig	Immunoglobulin
IHC	Immunohistochemistry
ITIM	Immunoreceptor tyrosine-based inhibition motif
ITP	Idiopathic thrombocytopenic purpura
IVIg	Intravenous infusion of gamma globulin
JCRB	Japanese Collection of Research Bioresources
K_D	Kinetics dissociation constant

L	Leucine
Leu	Leucine
mAb	Monoclonal antibody
MFI	Median fluorescent intensity
MPS	Mononuclear phagocytic system
MSX	Methionine sulfoximine
PBMC	Peripheral blood mononuclear cells
poAb	Polyclonal antibody
PT	Prothrombin time
SD	Standard deviation
TGI	Tumor growth inhibition
TIGIT	T cell immunoreceptor with Ig and ITIM domains
Tyr	Tyrosine
Y	Tyrosine

General Introduction

Historically, it is said that cancer has already been found around 1600 BC, and nowadays, cancer is the most common human genetic disease. Cancer cells can be generated in any organs and cell types. In normal conditions, cells are growing and proliferating to establish healthy human tissues and organs. There are over 1,000 gene mutations happening every day, however, there are also many check-points to detect those mutated genes to correct them to normal genes. If cells cannot modify those mutated genes to normal, those cells are killed or undergone to apoptosis by self-immune systems. In other words, normal cells are well-controlled to maintain themselves healthy. Cancer cells have multiple mutated genes and up- or down-regulated genes because of those mutation, resulted in uncontrolled overgrowth. In many cases, cancer cells over-express genes, like transforming growth factor-α (TGF-α), epidermal growth factor (EGF) and its receptor (EGFR), and vascular endothelial growth factor (VEGF) and its receptor (VEGFR) (Ciardiello et al., 2006). TGF-α and EGF pathways are important for the cancer development and progression. Therefore, the blockade of those pathways has already been candidates for anti-cancer therapy (Fox et al., 1994; Fan et al., 1998). VEGF pathway has been found as one of regulators of angiogenesis, and VEGF is secreted by cancer cells to stimulate blood vessels to cancer tissues (Ferrara et al., 1995). Bevacizumab (Avastin) is one of anti-VEGF antagonist antibody widely used for cancer treatment, and the clinical result of Bevacizumab promises that angiogenesis plays a key role for cancer cell survival and that angiogenesis inhibitors can be a potent anti-cancer therapy (Ferrara et al., 2005).

In general, cancer patients are treated with chemotherapies, targeted therapies, surgeries, and radio therapies depending on their cancer types, tissues and stages (Waks et al., 2019). There are many kinds of chemotherapies available, however, most of them

target rapid growth cells. Therefore, those chemotherapies affect growing cells in hair, skin, gut, bone marrows and others, and induce severe side effects, like hair loss, illness, bleeding, constipation and diarrhea. In contrast, targeted therapies are widely developing and used for cancer patient treatment. Targeted therapy works by targeting the cancer's specific genes, proteins, or tissue environment that contributes to cancer growth and survival. It is also well-known that targeted therapies cause less side effects compared with traditional chemotherapy since those do not affect other cells, which do not express target molecules. There are several types of targeted therapy, small molecule drugs and monoclonal antibodies. Traditional chemotherapies are also small molecules, however, small molecules used as targeted therapies target proteins and others to agonize/antagonize those functions. Erlotinib, for example, is widely used for non-small cell lung cancer treatment. Erlotinib, one of tyrosine kinase inhibitors, binds to intracellular of EGFR and blocks phosphorylation of EGFR induced by the binding of EGF (Dowell et al., 2005). As well as Erlotinib, Cetuximab is also a one of the most common cancer patient treatment as a targeted therapy (Maron et al., 2018). Cetuximab is a human antibody and binds to EGFR extracellular domain to inhibit EGF binding. Both small molecules and large molecules, like antibody therapy, as targeted therapy have positive features and negative features (Wan, 2016). Especially antibody therapeutics are widely used in multiple indications due to the stability, high binding activity and specificity.

Antibody, also as known as immunoglobulin (Ig), is a large Y-shaped protein produced by plasma cells, and is used to neutralize pathogens such as pathogenic bacteria and viruses. In human, there are five isotypes of antibody, IgG, IgM, IgA, IgD, and IgE. Most of antibodies have similar structures, two heavy chains (~50 kDa) and

two light chains (~25 kDa) connected by disulfide bonds. Fragment antigen-binding (Fab) is composed of one constant and one variable domain from each heavy and light chain of the antibody located in the N-terminus. The diversities of the antigen-binding are from diverse germline gene repertoires of the sequence in Fab regions. Also, it is said that the antibody binding to target is based on Fab sequences in heavy chain and the binding affinity is depending on the sequences on Fab in light chain. Two Fabs are connected to one Fc region corresponding to two heavy chains via the hinge region. This Fc region is the critical residues for the interaction with Fc gamma receptors (FcγRs) and complements in serum. FcγRs are widely expressed on multiple immune cells, such as T cells, NK cells, monocytes, macrophages, neutrophils, eosinophils and dendritic cells. Depending on the FcγRs binding to antibody, immune cells are activated and induce cytotoxic effects to the target. Especially in cancer, the antibody therapeutics induce antibody-dependent cellular cytotoxicity (ADCC) through the Fc binding to FcγRIIIa on NK cells (Wang et al., 2015). NK cells are activated via FcγRIIIa and secret granules, which is cytotoxic molecules and kill antibody-bound cancer cells. The target-bound antibody is also able to bind to FcγRI on macrophages and induce antibody-dependent cell-mediated phagocytosis (ADCP) to remove cancer cells like pathogens (Gül et al., 2015). In addition, complement components activate and form the membrane attack complex through cancer cell-bound antibody via Fc region to induce complement-dependent cytotoxicity (CDC). This antibody Fc region engages the MHC class I related receptor, FcRn, which enables antibody recycle, resulting in the blood half-life extension of antibodies (Ober et al., 2001). Thus, antibody therapeutics in cancer have not only target binding to agonize/antagonize its function, but also multiple effector functions to damage cancer cells. These specificity, high binding activity,

multiple functions and longer blood half-life make antibody therapeutics superiority compared with other small molecules. In addition to naked antibody therapeutics, multiple conjugations on antibody have been gaining momentum in these years. The conjugations include cytotoxic small molecules, radionuclides, and proteins (Beck et al., 2017; Mattes, 2002; Alewine et al., 2015, respectively). Those conjugated antibody therapeutics first bind to the target expressed on cancer cell surface and are internalized by endocytosis. In endosome, antibody conjugated with modality, such as cytotoxic small molecule, is degraded and the conjugated molecule is released from antibody in the form of active drug to induce cytotoxicity (Iamele et al., 2015).

Another important cancer therapy utilizing antibody therapeutics is the blockade of immune checkpoints to activate therapeutic anti-tumor immunity. Immune checkpoints are regulators of the immune systems and are crucial for self-tolerance, which prevent autoimmunity under normal conditions. Normal cells express immune checkpoint molecules, such as PD-L1, CD80, and B7 family proteins, to suppress cytotoxic T lymphocyte functions. Cancer cells also express those molecules on their surface, therefore, immune cells cannot distinguish cancer cells and normal cells. The idea of immune checkpoint inhibitors for cancer are to block this immune checkpoint suppressive pathway by antibodies to make cytotoxic T lymphocytes attacking cancer cells. The blockade of CTLA-4 and PD-1 pathways, that were recognized with the 2018 Nobel Prize in Physiology or Medicine awarded to James Allison and Tasuku Honjo, have achieved notable benefit in a variety of cancer treatment (Leach et al., 1996; Ishida et al., 1992). This kind of novel approach to activate self-immune system by antibody therapeutics will be significant therapeutic tools for the treatment of cancer patients.

The objective of this study was to identify a novel target for cancer patient treatment and to discover antibody therapeutics targeting it. I have discovered novel over-expressing membrane target molecule, Nectin-2, thorough gene-chip analysis and immunohistochemistory (IHC) in the study described in Chapter 1. I have also studied fully human antibodies against Nectin-2 with the evaluation of those antibodies in multiple biological function analysis in the same study. In the study described in Chapter 2, I have investigated anti-Nectin-2 monoclonal antibody in monkey toxicological experiments and found the adverse effect. I have applied Fc mutations to the antibody to mitigate the adverse effect and successfully discovered novel Fc mutated antibody, which demonstrated diminished side-effect in monkey with maintaining anti-tumor activity through ADCC in mouse xenograft models.

Chapter 1:

Nectin-2 is a Potential Target for Antibody Therapy of Breast and Ovarian Cancers

Abstract

Nectin-2 is a Ca^{2+}-independent cell-cell adhesion molecule that is one of the plasma membrane components of adherens junctions. However, little is reported about the involvement of Nectin-2 in cancer. I found that Nectin-2 was over-expressed in clinical breast and ovarian cancer tissues by gene expression profile analysis and immunohistochemistry studies. Nectin-2 was over-expressed in various cancer cell lines, too. Furthermore, polyclonal antibody specific to Nectin-2 suppressed *in vitro* proliferation of OV-90 ovarian cancer cells endogenously expressing Nectin-2 on cell surface. I generated 256 fully human anti-Nectin-2 monoclonal antibodies (mAbs), which were classified into 7 epitope bins. The anti-Nectin-2 mAbs demonstrated antibody-dependent cellular cytotoxicity (ADCC) and epitope bin-dependent features such as inhibition of Nectin-2 *trans*-interaction and *in vitro* cancer cell proliferation. A representative anti-Nectin-2 mAb in epitope bin VII, Y-443 showed anti-tumor effect against OV-90 cells and MDA-MB-231 breast cancer cells in mouse therapeutic models, and its main mechanism of action appeared to be ADCC. Those findings strongly suggest Nectin-2 is a potential target of antibody therapy for breast and ovarian cancers.

Introduction

Nectins are Ca^{2+}-independent cell adhesion molecules that consist of four members: Nectin-1, -2, -3, and -4. Each member of the Nectin family except for Nectin-4 has two or three splicing variants (Takai et al., 2003). All members except for a secreted protein Nectin-1γ have an extracellular region that contains three immunoglobulin (Ig)-like domains, a single transmembrane region, and a cytoplasmic region. Nectins form homo-*cis*-dimers on the cell surface via Ig2-domain (Momose et al., 2002). The *cis*-dimers further form homo- and hetero-*trans*-dimers with other *cis*-dimers of Nectins on adjacent cells via the Ig1-domain (Lopez et al., 1998; Satoh-Horikawa et al., 2000; Miyahara et al., 2000; Reymond et al., 2001; Momose et al., 2002; Fabre et al., 2002; Yasumi et al., 2003).

Nectin-2 has been reported to regulate cell adhesion between epithelial cells through the formation of *trans*-dimers between adjacent cells (Takai et al., 2003). Nectin-2-mediated cell adhesion induces the formation of E-cadherin-based adherens junctions followed by the formation of claudin-based tight junctions (Fukuhara et al., 2002a; Fukuhara et al., 2002b; Fukuhara et al., 2003; Morita et al., 2010). In addition to its function as a cell adhesion molecule, previous studies have suggested that Nectin-2 acts as an organizer of Sertoli cell-spermatid junctions in the testis (Bouchard et al., 2000) and of synapse formation by neurons (Mizoguchi et al., 2002; Inagaki et al., 2003), and as an entry receptor for viruses (Warner et al., 1998). Nectin-2 is also known to be one of the ligands of DNAM-1 and TIGIT (T cell immunoreceptor with Ig and ITIM domains) (Bottino et al., 2003; Takahara-Hanaoka et al., 2004; Stanietsky et al., 2009; Chan et al., 2012). Although anti-Nectin-2 antibodies have been examined from a functional

perspective such as for the inhibition of Nectin-2 binding to DNAM-1, *in vitro* cell aggregation or HSV-1 virion-induced cell fusion into host cells (Lopez et al., 1998; Takahara-Hanaoka et al., 2004; Aoki et al., 1997; Delboy et al., 2006), there is no report that has showed the anti-tumor effect of anti-Nectin-2 antibody. In this chapter, I sought to clarify the expression profile of Nectin-2 in various cancers. In addition, anti-Nectin-2 mAb demonstrated *in vivo* anti-tumor effect on breast and ovarian cancer cell lines, suggesting potential of Nectin-2 as a target of antibody therapy for cancer treatment.

Materials and Methods

Plasmid Construction

Nectin-2 was cloned from Marathon-Ready cDNA of the A549 human lung cancer cell line (BD Biosciences) into mammalian expression vectors pcDNA3.1 (Invitrogen), pEE12.4 (Lonza Biologics) or pEF1/myc-HisA (Invitrogen) to obtain pcDNA3.1-Nectin-2, pEE12.4-Nectin-2 or pEF1/myc-HisA-Nectin-2, respectively. The cDNA encoding human IgG_1 and IgG_4 Fc region and mouse IgG_{2a} Fc region were cloned from human spleen-derived and mouse spleen-derived Marathon-Ready cDNA (BD Biosciences), respectively. The cDNA encoding Nectin-2 extracellular domain (a.a. 1–361) fused to the human IgG_1 Fc region and Nectin-3 extracellular domain (a.a. 1–404) fused to the mouse IgG_{2a} Fc region were inserted into pcDNA3.1 (Invitrogen) to obtain pcDNA3.1-Nectin-2-ED-hFc and pcDNA3.1-Nectin-3-ED-mFc plasmids, respectively. Similarly, the cDNA encoding C-terminal FLAG-tagged Nectin-2 extracellular domain (a.a. 1–361) and Nectin-3 extracellular domain (a.a. 1–404) were inserted into the pCMV-Tag4a plasmid (Stratagene) to obtain pCMV-Tag4-Nectin-2-ED-FLAG and pCMV-Tag4-Nectin-3-ED-FLAG plasmids, respectively. To obtain an expression plasmid encoding Y-443 with the human IgG_4 Fc region, cDNA of the variable regions of the heavy chain or light chain of Y-443 were inserted into the GS expression vector pEE6.4 (Lonza Biologics) with human IgG_4 Fc region cDNA or pEE12.4 (Lonza Biologics), respectively. The Y-443 IgG_4 expression vector was constructed by ligation of the heavy and light chain vector.

Cells

OV-90 and MDA-MB-231 cells were purchased from the American Type Culture Collection (ATCC). OV-90 cells were grown in a 1:1 mixture of MCDB 105 medium and Medium 199 containing 15% fetal bovine serum (FBS). MDA-MB-231 cells were grown in Leibovitz's L-15 medium containing 10% FBS. FM3A (Health Protection Agency Culture Collections (HPACC)) cells were grown in RPMI1640 containing 10% FBS. CHO (Lonza Biologics) and NS0 cells (Lonza Biologics) were cultured in DMEM containing 10% dialyzed FBS. The other cancer cell lines for Nectin-2 expression tests for FCM analysis were purchased from the ATCC, the German Collection of Microorganisms and Cell Cultures (DSMZ), the Japanese Collection of Research Bioresources Cell Bank (JCRB), and HPACC, and were cultured according to the provider's instructions.

To obtain Nectin-2 stable transfectants, pEF1/myc-HisA-Nectin-2 was transfected into FM3A cells by using a Gene Pulser II (Bio-Rad). The cells were cultured in 96-well plates with selection medium containing Geneticin (Life Technologies). Likewise, pEE12.4/Nectin-2 was transfected into CHO and NS0 cells using a Gene Pulser II (Bio-Rad). The transfected cells were cultured in 96-well plates with selection medium containing methionine sulfoximine and L-glutamine-free selection medium, respectively. Single colonies grown in the selection media were expanded and the expression level of Nectin-2 on the cell surface was measured by FCM using anti-Nectin-2 polyclonal antibody (poAb). Thus, recombinant cell lines expressing Nectin-2 (Nectin-2/FM3A, Nectin-2/CHO and Nectin-2/NS0) were obtained.

Recombinant Protein Preparation

Recombinant protein Nectin-2-ED-FLAG or Nectin-3-ED-FLAG were

transiently expressed in FreeStyle 293F cells (Life Technologies) by transfecting pCMV-Tag4-Nectin-2-ED-FLAG or pCMV-Tag4-Nectin-3-ED-FLAG using 293fectin (Life Technologies), respectively. The Nectin-2-ED-FLAG and Nectin-3-ED-FLAG proteins were then purified from the culture supernatant by anti-FLAG antibody column chromatography (Sigma-Aldrich) followed by a buffer exchange with Dulbecco's phosphate-buffered saline (D-PBS) using an ultra-filtration system (Amicon). Similarly, recombinant protein of Nectin-2-ED-hFc or Nectin-3-ED-mFc was obtained by the transfection of pcDNA3.1-Nectin-2-ED-hFc or pcDNA3.1-Nectin-3-ED-mFc, respectively. The Nectin-2-ED-hFc and Nectin-3-ED-mFc proteins were purified from the culture supernatant with Protein A Sepharose (GE Healthcare), followed by a buffer exchange with D-PBS using an ultra-filtration system.

Anti-Nectin-2 Polyclonal Antibody

Anti-Nectin-2 poAb was raised in New Zealand white rabbits by immunizing recombinant Nectin-2-ED-FLAG protein emulsified with Freund's adjuvant every 2 weeks several times. The anti-Nectin-2 poAb was purified from the antiserum by affinity chromatography using a HiTrap NHS-Activated HP column (GE Healthcare) on which Nectin-2-ED-FLAG was immobilized. The purified antibodies were then passed through a Nectin-3-ED-FLAG-affinity column in order to remove antibodies that were cross-reactive to Nectin-3 or FLAG tag. The flow through fraction was used as a Nectin-2-specific poAb.

mRNA Expression Analysis

Expression levels of Nectin-2 mRNA in normal tissues and cancer tissues were

quantified by analyzing Affymetrix U_133 array data from Gene Logic. Nectin-2 mRNA level was calculated by multiplying each expression intensity for a given experiment (a sample hybridized onto a chip) by a global scaling factor. The scaling factor was calculated as follows: (1) from all the unnormalized expression values in the experiment, the largest 2% and smallest 2% of the values were deleted; (2) the mean of the remaining values (trimmed mean) was calculated; (3) the scale factor was calculated as 100/(trimmed mean). The value of 100 used here is the standard target value used by Gene Logic. A genechip probe 232078_at for human Nectin-2 was used for the analysis. Primary cancer tissues were used in the analysis as cancer tissues.

IHC

The expression level of Nectin-2 protein in tissues was examined by IHC using paraffin-embedded normal tissue sections and cancer tissue sections from cancer patients (Cybrdi). The tissue sections were deparaffinized, blocked with goat serum (Vector Laboratories) for 20 min at room temperature, and incubated with 1 μg/ml anti-Nectin-2 poAb for 18 h at 4ºC. After three washes with D-PBS, the tissue sections were incubated with ENVISION+ Rabbit/HRP (Dako) for 30 min and then developed with 3, 3'-diaminobenzidine for 3 min at room temperature. The sections were counterstained with hematoxylin and mounted in Permount (Fisher Scientific). Cases with membranous staining in tumor cells were considered to be positive for Nectin-2 expression. The antigen-specificity of the positive samples was confirmed by staining without anti-Nectin-2 primary antibody.

FCM

Cancer cells were incubated with 3 μg/ml anti-Nectin-2 rabbit poAb for 1 h on ice followed by incubation with 2 μg/ml Alexa488-labeled anti-rabbit IgG (Life Technologies) for 1 h on ice. Cells were washed with D-PBS containing 2% FBS after each antibody incubation step. The fluorescence intensity was measured by using a Cytomics FC 500 instrument (Beckman Coulter). The MFI ratio of the Ab-treated sample to a control sample was used as a measurement of the cell surface expression level of Nectin-2 in cancer cells. A control sample was prepared by incubating cells with a rabbit IgG control (Jackson ImmunoResearch Laboratories).

Generation of Fully Human Anti-Nectin-2 mAbs

KM mice (10–12-weeks old, male; Kyowa Hakko Kirin) were immunized with Nectin-2-expressing cells (Nectin-2/NS0 or Nectin-2/FM3A), a recombinant protein of Nectin-2 extracellular domain (Nectin-2-ED-hFc or Nectin-2-ED-FLAG) or a combination of Nectin-2/FM3A and the recombinant protein. For cell immunization, Nectin-2/NS0 or Nectin-2/FM3A cells were pre-treated with 20 μg/ml Mitomycin C (Wako) for 30 min at 37ºC and then they were intraperitoneally injected into the mice with Ribi adjuvant at 1×10^7 cells per mouse weekly for 7 weeks. For protein immunization, an emulsion of 50 μg of Nectin-2-ED-hFc or Nectin-2-ED-FLAG and Freund's complete adjuvant (Difco) was subcutaneously injected into the KM mice. The following immunizations were repeated twice using the same amounts of immunogens emulsified with Freund's incomplete adjuvant at 2-wk intervals. Two weeks after the third immunization, 10 μg of Nectin-2-ED-hFc or Nectin-2-ED-FLAG was injected into the tail vein as a final boost. For combination immunization, the first immunization was conducted subcutaneously with Nectin-2-ED-hFc or Nectin-2-ED-FLAG emulsified with

Freund's complete adjuvant followed by the second immunization with the same amount of the proteins emulsified with Freund's incomplete adjuvant at 2-wk intervals. In parallel, Mitomycin C treated-Nectin-2/FM3A cells were intraperitoneally injected into the mice every week for 4 weeks after the first protein immunization. Three days after the final protein immunization or 7 days after the final cell immunization, splenocytes were collected from mice that showed a high serum titer against Nectin-2 in a cell ELISA using Nectin-2/CHO and they were fused with mouse myeloma P3X63Ag8U.1 cells (ATCC) using Polyethylene Glycol 1500 (Roche Diagnostics). The fused cells were cultured in a HAT (hypoxanthine-aminopterin-thymidine)-selection media to obtain hybridomas. Hybridomas that secreted anti-Nectin-2 mAb were screened in a Nectin-2/CHO cell ELISA using the culture supernatant. After the selected hybridomas were further sub-cloned, all of the hybridomas that secreted Nectin-2-specific antibody were expanded in medium containing 10% ultra-low IgG FBS (Life Technologies) at the 10 to 50 ml scale. Then, each mAb was purified from the culture supernatant using Protein A-Sepharose resin. Isotypes of the antibodies were determined by a sandwich ELISA using a plate that was separately coated with 6 different antibodies specific to human IgG_1, IgG_2, IgG_3, IgG_4, IgM or the kappa chain.

Epitope Binning Study

Anti-Nectin-2 mAbs were biotinylated by using a Biotin Labeling Kit-NH2 (Dojindo). Three thousands Nectin-2/CHO cells were pre-incubated with 5 μg/ml unlabelled anti-Nectin-2 mAb and 330 ng/ml Streptavidin-Alexa Fluor 647 (Life Technologies) in a 384-wel FMAT plate (Applied Biosystems) for 10 min at room temperature. After incubation, the biotinylated anti-Nectin-2 mAb was added to the plate

at a final concentration of 100 ng/ml and the plate was further incubated for 1 h at room temperature.

The fluorescence intensity of Alexa Fluor 647 on Nectin-2/CHO cells was detected by using a FMAT8200 Cellular Detection System (Applied Biosystems). The binding inhibition (%) was calculated using the following formula:

Binding inhibition (%) = $(1 - A/B) \times 100$

where A represents the total fluorescence of the added unlabeled antibody and B represents the total fluorescence in an unlabeled antibody-free well. An epitope binning study was performed with the binding inhibition data by employing Ward's hierarchical clustering method and using SpotFire DecisionSite for Lead Discovery (TIBCO Software).

Cell Proliferation Assay

OV-90 cells were seeded at 3 x 10^3 cells/well in a 96-well plate in the presence of 1% FBS and 30 μg/ml anti-Nectin-2 poAb or mAbs and then cultured for 6 days at 37ºC. Cell proliferation was measured by using a Cell Counting Kit-8 (Dojindo). The efficacy of the anti-Nectin-2 mAbs was evaluated with various concentrations of the antibodies under the same conditions. Cell growth inhibition (%) was calculated using the following formula:

Cell growth inhibition (%) = 100 × [1 – Absorbance450 (with Ab) / Absorbance450 (without Ab)]

Nectin-2 Trans-Interaction Inhibition Assay

Nectin-2-Nectin-3 *trans*-interaction inhibition was quantitatively assessed by

using a Biacore2000 (GE Healthcare). In brief, Nectin-3-ED-mFc protein was immobilized on sensor chip CM5 (GE Healthcare) by using an Amine Coupling Kit (GE Healthcare). Then, a mixture of Nectin-2-ED-hFc at 40 μg/ml and anti-Nectin-2 mAb at 30 μg/ml was passed through the Nectin-3-ED-mFc immobilized chip. Nectin-2-Nectin-3 *trans*-interaction inhibition was calculated as a percentage of the decrease in the maximum response unit compared to a human IgG control (Jackson ImmunoResearch Laboratories).

Nectin-2-Nectin-2 *trans*-interaction inhibition was measured by using an ELISA-based time-resolved fluorescence spectroscopy assay. Nectin-2-ED-hFc protein was conjugated with europium N1 ITC chelate by using a DELFIA Eu-Labeling Kit (PerkinElmer). Unlabeled Nectin-2-ED-hFc protein was immobilized on to a Delfia Clear Strip Plate (PerkinElmer). After blocking with PBS containing 2% bovine serum albumin, the Eu-labeled Nectin-2-ED-hFc and anti-Nectin-2 mAb were simultaneously added at final concentrations of 3.2 μg/ml and 30 μg/ml, respectively, followed by incubation for 1.5 h at room temperature. After washing with D-PBS containing 0.05% Tween20, Enhancement Solution (PerkinElmer) was added to each well. The fluorescence intensity was measured at 615 nm with an excitation wavelength of 340 nm and a delayed time of 400 μs by using an ARVO1420 Multilabel Counter (PerkinElmer). Nectin-2-Nectin-2 *trans*-interaction inhibition was calculated as a percentage of the decrease in the fluorescence signal compared to a human IgG control.

ADCC Assay

Human peripheral blood mononuclear cells (PBMC) from All Cells were cultured in RPMI1640 medium containing 10% FBS, 0.1 nM human IL-2 (DIACLONE

Research), and 55 μM 2-mercaptoethanol for 24 h. PBMC were incubated with ^{51}Cr-labelled OV-90 cells or ^{51}Cr-labelled MDA-MB-231 cells at a ratio of 50:1 in the presence of anti-Nectin-2 mAb for 4 h at 37ºC. After incubation, the radioactivity of ^{51}Cr that had been released into the culture medium from the target cells was measured by using an AccuFLEX γ 7000 (Aloka). Specific lysis by anti-Nectin-2 mAb was calculated using the following formula:

$$\text{Specific lysis (\%)} = 100 \times (A - B)/(C - B)$$

where A represents the radioactivity of the test supernatant, B represents the radioactivity of the target cells alone, and C represents the radioactivity of the maximum ^{51}Cr release from the target cells that were lysed with 1% Triton X-100.

CDC Assay

Five thousands of MDA-MB-231 cells were incubated with 10-fold diluted human serum complement (Quidel) and various concentrations of Y-443 in a black wall/transparent bottom 96-well plate (BD Biosciences) for 60 min at 37ºC. Cells were stained with 10 μM propidium iodide (PI). PI-positive cells (CDC-damaged cells) were detected using an Acumen ex3 instrument (TTP Labtech). As a positive control, rituximab (Roche) was used in combination with Daudi cells (ATCC). CDC activity was calculated using the following formula: $\text{CDC activity (\%)} = 100 \times (A - B)/(C - B)$

where A represents the number of PI-positive cells in the presence of mAb and human serum, B represents that in the absence of mAb, and C represents the number of PI-positive cells that were incubated with 0.1% Triton X-100.

Preparation of Anti-Nectin-2 mAbs for In Vivo Study

The hybridomas that produced Y-187 and Y-443 were cultured in Daigo's T medium (Nihon Pharmaceutical) containing 10% Ultra Low IgG FBS (Life Technologies). The culture supernatant was filtered, concentrated, and then purified with a Protein A-column. The antibody fraction was separated on a Superdex 200 26/60 column (GE Healthcare) to obtain the monomer fraction and endotoxins were removed by using an ActiClean Etox column (Sterogene). The recombinant IgG_4 form of Y-443 was prepared as follows. CHOK1SV cells (Lonza Biologics) were maintained in CD-CHO medium (Life Technologies) containing 6 mM L-glutamine. Linearized Y-443 IgG_4 expression vector was transfected into CHOK1SV cells with a Gene Pulser II. The cells were seeded into 96-well plates at 37°C in a humidified 8% CO_2. After 1 day of culturing, methionine sulfoximine (MSX) was added at a final concentration of 25 μM. After selection of the culture, a recombinant CHOK1SV clone that produced high levels of Y-443 IgG_4 was selected and the cells were expanded into T75 flasks in serum-free CD-CHO medium containing 25 μM MSX and then adapted into a suspension culture. Y-443 IgG_4 was purified from the supernatant of a 1 L fed-batch culture by chromatography with Protein A Sepharose FF (GE Healthcare), followed by Superdex200 26/60.

In Vivo Study

For the OV-90 subcutaneous mouse xenograft model, 8×10^6 OV-90 cells were subcutaneously inoculated into a flank of BALB/cAJcl-nu/nu mice (6-weeks old, females) from CLEA Japan. Then, the mice were randomly grouped (n = 13-17). Vehicle (D-PBS), Y-187 or Y-443 (15 mg/kg) was intravenously injected twice weekly for 5 weeks from the day of the cancer cell inoculation. Tumor diameters were measured with a caliper twice weekly and approximate tumor volumes were calculated as 0.5 × length ×

(width)^2 during the treatment period to monitor tumor growth. The TGI (TGI) was calculated by the following formula:

$$TGI = 100 \times (1 - A/B)$$

where A is the average tumor volume for the Ab-treated group and B is the average tumor volume for the vehicle group. The difference in the average tumor volume between the Ab-treated groups and the vehicle group was analyzed using the Steel test.

For the MDA-MB-231 subcutaneous xenograft model, 3×10^6 of MDA-MB-231 cells were subcutaneously inoculated with Matrigel (Becton Dickinson) into BALB/cAJcl-nu/nu mice (6-weeks old, female) as described above. The mice were grouped on 36 days after the inoculation when the average sizes of the tumors reached approximately 200 mm^3 and then vehicle (D-PBS), Y-443 (0.3 and 1 mg/kg) or its IgG_4 form antibody (0.3, 1, and 3 mg/kg) was intravenously injected weekly three times. The tumor volumes were measured and the TGI for each treatment group was determined at day 57 as described above. The difference in the average tumor volume between the Ab-treated groups and the vehicle group was analyzed using Williams test.

The MDA-MB-231 lung metastasis model was carried out as follows. Briefly, 100 μl of 1×10^6 cultured MDA-MB-231 cancer cell suspension in Hank's buffered salt solution was intravenously injected into the tail vein of SCID mice (5-6 weeks old). The mice were randomly grouped (n = 5) 33 days after the inoculation and were treated with vehicle (D-PBS) or Y-443 (0.001, 0.01, 0.1, 1, or 10 mg/kg) weekly on days 33, 40, 47, and 54. On day 61, the mice were sacrificed to excise the lungs, and 0.2% Evans blue dye was injected intratracheally to visualize their tumor colonies. The lungs were subsequently fixed with a mixture of picric acid,10% neutral buffered formalin, and acetic acid (15:5:1), and the number of colonies on the diaphragmatic surface of the lungs was

counted macroscopically in a blind manner. The difference between the colony numbers of the Ab-treated group and the vehicle group was analyzed using the one-tailed Shirley-Williams test. TGI was calculated by using the following formula:

$$TGI = 100 \times (1 - A/B)$$

where A is the average colony number for the Ab-treated group and B is the average colony number for the vehicle group.

Ethics statement

All of the animal studies including immunization were carried out in strict accordance with the recommendations in the Guide for the Care and Use of Laboratory Animals of the National Institutes of Health. The protocol was approved by the Committee on the Ethics of Animal Experiments of Takeda Pharmaceutical Company Ltd. (Permit Numbers: 2802, 2701, and E1-0311).

Results

Over-expression of Nectin-2 in Breast and Ovarian Cancers

With the aim of identifying target proteins for antibody therapeutics, I searched for membrane-bound proteins that were over-expressed in cancer tissues compared to normal tissues using Affymetrix GeneChip Technology and found that Nectin-2 mRNA was over-expressed in various cancer tissues. An analysis that compared the mean intensity in each tissue set demonstrated that Nectin-2 was especially over-expressed in breast, ovarian, and prostate cancer tissues (Figure 1). I subsequently confirmed the over-expression of Nectin-2 protein in breast and ovarian cancer tissues by immunohistochemistry (IHC), and then found that Nectin-2 protein was abundantly present in these cancer tissues while it was undetectable in normal breast and ovary tissues (Figure 2). A more extensive IHC study indicated that Nectin-2 protein was over-expressed in more than 80% of breast cancer tissue samples and about 50% of ovarian cancer tissues samples (Table 1). On the other hand, Nectin-2 was expressed only in the liver and testis within normal tissue specimens (Table 2). Furthermore, Nectin-2 was broadly over-expressed in various breast and ovarian cancer cell lines when its expression was tested by FCM analysis using anti-Nectin-2 poAb (Figure 3). I selected OV-90 ovarian cancer cells that highly expressed Nectin-2 with a median fluorescent intensity (MFI) of 242 in FCM and MDA-MB-231 breast cancer cells (MFI = 181) for the evaluation of anti-Nectin-2 antibodies in *in vitro* assays and *in vivo* studies.

Generation of Fully Human Anti-Nectin-2 mAbs

I generated fully human anti-Nectin-2 mAbs by a conventional hybridoma

technology using KM mice that carried the complete locus for the human immunoglobulin heavy chain and a transgene for the human immunoglobulin kappa light chain (Tomizuka et al., 2000). I immunized the KM mice with a recombinant protein of the Nectin-2 extracellular domain and/or recombinant Nectin-2 over-expressing cells. As a result of the immunization and screening by a cell enzyme-linked immunosorbent assay (ELISA) using Nectin-2/CHO cells, 256 hybridoma clones that secreted human anti-Nectin-2 mAbs were established. The IgG mAbs were purified from a small scale culture of the hybridomas and were used for characterization.

I selected 185 out of 256 mAbs that showed relatively higher binding affinity to Nectin-2/CHO cells in the cell ELISA for an epitope binning analysis. Binding of biotinylated anti-Nectin-2 mAbs to the recombinant CHO cells that over-expressed Nectin-2 were measured in the absence and presence of an excess amount of unlabelled anti-Nectin-2 mAbs. Based on the percentage of competitive binding inhibition for each combination of antibodies, I classified the mAbs into 7 major bins (I to VII) by a clustering analysis method using Spotfire DecisionSite for Lead Discovery (Figure 4).

Inhibitory Activities of Anti-Nectin-2 antibodies on the *in vitro* Proliferation of OV-90 Cancer Cells

Although I found that Nectin-2 was over-expressed in various types of cancers, there was no report suggesting the involvement of Nectin-2 in cancer cell proliferation. In order to investigate the potential of Nectin-2 as a target for antibody therapies of cancers, I generated anti-Nectin-2 rabbit poAb using a recombinant Nectin-2 protein as an immunogen. The anti-Nectin-2 poAb at 30 μg/ml inhibited the cell proliferation of OV-90 ovarian cancer cells by 10-15 % (Figure 5). Although the percentage of the cancer

cell growth inhibition was insignificant, the suppression was reproducible.

I next screened the 256 anti-Nectin-2 mAbs in the cell proliferation assay. The 30 mAbs, which had shown certain growth inhibition activities against OV-90 cells in the first screening, were retested in the same assay and 8 of them reproducibly inhibited cell proliferation (Figure 5). All 8 clones (Y-052, Y-047, Y-125, Y-137, Y-187, Y-205, Y-214, and Y-226) inhibited OV-90 cell proliferation in a concentration-dependent manner. Seven out of the 8 mAbs besides Y-052 belonged to epitope bin VI (Figure 5). The concentration-dependent inhibitory activity of the representative mAb Y-187 on OV-90 cell proliferation is shown in Figure 6 as an example.

Inhibitory Activity of Anti-Nectin-2 mAbs on Nectin-2 *Trans*-Interaction

As a cell adhesion molecule, Nectin-2 forms a *cis*-dimer and then interacts with another Nectin-2-*cis*-dimer or Nectin-3-*cis*-dimer on adjacent cells to form a homo-*trans*-dimer or hetero-*trans*-dimer, respectively (Lopez et al., 1998; Satoh-Horikawa et al., 2000; Miyahara et al., 2000; Reymond et al., 2001; Fabre et al., 2002; Momose et al., 2002; Yasumi et al., 2003). Previous reports showed that some anti-Nectin-2 antibodies inhibited cell aggregation (Aoki et al., 1997; Lopez et al., 1998). However, there was no report that measured the effect of anti-Nectin-2 antibody separately on Nectin-2-Nectin-2 and on Nectin-2-Nectin-3 *trans*-binding. I therefore examined whether anti-Nectin-2 mAbs could inhibit Nectin-2-Nectin-2 or Nectin-2-Nectin-3 *trans*-interaction which mimics the *trans*-binding of the Nectins between cells using ELISA-based or Biacore-based assays, respectively. As summarized in Figure 7, most of the mAbs in epitope bins V and VI inhibited both Nectin-2-Nectin-2 and Nectin-2-Nectin-3 *trans*-interaction. Interestingly, the mAb in epitope bin V inhibited Nectin-2-Nectin-2 *trans*-interaction

more strongly than the mAbs in epitope bin VI. Inverse to this, the mAbs in epitope bin VI except Y-232 inhibited Nectin-2-Nectin-3 *trans*-interaction more strongly than the mAbs in epitope bin V. The anti-Nectin-2 mAbs in epitope bins I and IV weakly inhibited *trans*-interaction and the mAbs in epitope bin VII showed no inhibition of Nectin-2-Nectin-2 nor Nectin-2-Nectin-3 *trans*-interaction. Thus, the inhibitory activities of anti-Nectin-2 mAbs on Nectin-2 *trans*-interaction were epitope bin-dependent.

ADCC of Anti-Nectin-2 mAbs on OV-90 Cancer Cells

ADCC is one of the mechanisms of action of marketed therapeutic antibodies such as rituximab and trastuzumab (Clynes et al., 2000), and that IgG_1 antibodies demonstrate the most potent ADCC among human IgG isoforms (Steplewski et al., 1988). In order to evaluate the epitope bin-dependency of anti-Nectin-2 mAbs for ADCC, I selected a few IgG_1 antibodies with similar antigen-binding affinity (EC_{50} in Cell ELISA ranging from 0.22 to 0.59 nM with the exception of Y-278 which EC_{50} was 2.1 nM) from each epitope bin and measured the ADCC against OV-90 cells. Although the specific cell lysis was saturated at around 30% by a technical reason, all of the anti-Nectin-2 mAbs tested showed ADCC against OV-90 cells in a concentration-dependent manner. The concentration giving 15% specific cell lysis varied from 0.01 to 1 μg/ml, and interestingly, all of the three anti-Nectin-2 mAbs in epitope bin VII (Y-055, Y-414, and Y-443) showed the highest potency within the mAbs (Figure 8).

Anti-Tumor Effect of Anti-Nectin-2 mAbs against OV-90 Cancer Cells in a Mouse Subcutaneous Xenograft Model

To see if the anti-Nectin-2 mAbs exerted *in vivo* anti-tumor effects, I selected

two representative mAbs, Y-187 from epitope bin VI and Y-443 from epitope bin VII, which showed different biological activities. Namely, Y-187 inhibited Nectin-2-Nectin-3 *trans*-interaction and *in vitro* OV-90 cell proliferation and showed ADCC against OV-90 cells (Figure 5-8). On the other hand, Y-443 did not inhibit Nectin-2-*trans*-interaction nor *in vitro* OV-90 cell proliferation but showed ADCC (Figure 5, 7, and 8). In a subcutaneous mouse xenograft preventive model, intravenous administrations of both Y-187 and Y-443 (15 mg/kg twice a week) remarkably inhibited OV-90 tumor growth by 93% and 92%, respectively (Figure 9).

Anti-Tumor Effect of Y-443 against MDA-MB-231 Breast Cancer Cells in a Mouse Lung Metastasis Model

Since the inhibition of the Nectin-2 function as a cell adhesion molecule may cause adverse effects, I focused on Y-443, which did not inhibit Nectin-2-Nectin-2 or Nectin-2-Nectin-3 *trans*-interaction (Figure 7), and further evaluated its anti-tumor effect on MDA-MB-231 breast cancer cells in an established mouse lung metastasis model. I started dosing the antibody at the time when the colonies of MDA-MB-231 cells became visible in the lungs. As shown in Figure 10, Y-443 dose-dependently suppressed the growth of MDA-MB-231 cells in lungs with tumor growth inhibition (TGI) of 28%, 49%, 74%, 65%, and 71% for 0.001, 0.01, 0.1, 1, and 10 mg/kg group, respectively. The minimum effective dose of Y-443 for this experimental condition was 0.1 mg/kg.

Mechanism of Action of the *in vivo* Anti-Tumor Effect of Y-443

The differences in the *in vitro* characteristics of Y-187 and Y-443 and the similarities in anti-tumor effects on OV-90 cells described above suggested that the anti-

tumor effects of these two mAbs were not dependent on *in vitro* inhibitory activities against cell proliferation, Nectin-2-Nectin-2 nor Nectin-2-Nectin-3 interaction, but most likely dependent on ADCC. In order to confirm this, I prepared recombinant Y-443 IgG_4 antibody in which the IgG_1 Fc region of Y-443 was swapped for IgG_4 Fc since IgG_4 isoform is known to have much less ADCC activity (Steplewski et al., 1988). The binding activity of Y-443 IgG_4 against Nectin-2 was equivalent to that of the IgG_1 isoform (K_D = 2.9 nM and 3.0 nM, respectively). Y-443 (IgG_1) showed potent ADCC against MDA-MB-231 cells and the ADCC disappeared as a result of Fc-conversion to IgG_4 (Figure 11). In a mouse subcutaneous xenograft established model that carries the same breast cancer cells, the TGIs of Y-443 (IgG_1) at 0.3 and 1 mg/kg were 65% and 53%, respectively (Figure 12). On the other hand, the TGIs of Y-443 IgG_4 at 0.3, 1, and 3 mg/kg were 39%, 31%, and 39%, respectively. Thus, Y-443 IgG_4 at 3 mg/kg showed less anti-tumor effect than Y-443 (IgG_1) at 0.3 mg/kg.

Tao et al. reported that IgG_1 but not IgG_4 isoform could exert complement-dependent cytotoxicity (CDC) as an effector function (Tao et al., 1991). Therefore, I investigated the contribution of CDC in anti-tumor effect of Y-443(IgG_1). However, as shown in Figure 13, Y-443(IgG_1) did not show CDC against MDA-MB-231 cells at all, whereas rituximab showed marked CDC against Daudi cells in the similar conditions. These results suggest that the *in vivo* anti-tumor effect of the anti-Nectin-2 mAb was mainly attributed to ADCC.

Discussion

The over-expression of Nectin-2 in breast and ovarian cancer tissues and various cancer cell lines at the mRNA as well as protein levels (representative data was shown in Figures 1 and 2 and Tables 1 and 2) suggests the potential of Nectin-2 as a target for antibody therapeutics to treat patients that are afflicted with these cancers. In addition, the over-expression of Nectin-2 in cell lines derived from various type of cancers (Figure 3) and in neuroblastoma, myeloid, lymphoblastic leukemia, gastric cancer and colon cancer (Castriconi et al., 2004; Pende et al., 2005; Tahara-Hanaoka et al., 2006) suggests the possibility for the application of anti-Nectin-2 antibody to treat various cancer types.

Since a partial growth inhibition of OV-90 ovarian cancer cells had been observed by anti-Nectin-2 poAb, I generated 256 Nectin-2-specific fully human mAbs from KM mice. The mAbs were classified into mainly 7 epitope bins by a competitive binding inhibition method using recombinant CHO cells that over-expressed Nectin-2 (Figure 4). In this assay format, the two antibodies binding to the epitopes that were not identical but close to each other could also competitively bind to Nectin-2 due to steric hindrance and were classified into the same epitope bin. Therefore, the number of epitope bins for anti-Nectin-2 mAbs might have been underestimated.

In the Nectin-2-Nectin-3 *trans*-interaction assay, 73 out of the 78 neutralizing mAbs belonged to epitope bin V or VI (representative data was shown in Figure 7). Interestingly, these mAbs failed to bind to a Nectin-2 Ig1 domain deletion mutant, whereas they retained the ability to bind to a Nectin-2 Ig2 domain deletion mutant (data not shown). These results suggest that the epitopes of the antibodies in epitope bins V and VI were located in the Ig1 domain, which has been reported to be responsible for the

formation of the Nectin's *trans*-interaction (Lopez et al., 1998; Satoh-Horikawa et al., 2000; Miyahara et al., 2000; Reymond et al., 2001; Fabre et al., 2002; Momose et al., 2002; Yasumi et al., 2003). Moreover, it is noteworthy that Nectin-2-Nectin-2 *trans*-interaction was inhibited more strongly by the antibodies in epitope bin V, whereas Nectin-2-Nectin-3 *trans*-interaction was inhibited more strongly by the antibodies in epitope bin VI (Figure 7). These findings suggest that the interaction sites for the hetero-*trans*-interaction and homo-*trans*-interaction of the Ig1 domain of Nectin-2 are not completely identical, which may enable Nectin-2-Nectin-2 *trans*-dimer and Nectin-2-Nectin-3 *trans*-dimer to multimerize with each other.

Anti-Nectin-2 mAbs representing each epitope bin with similar antigen binding affinity showed various ADCC activities, and the mAbs in epitope bin VII demonstrated the strongest ADCC (Figure 8). Interestingly, a subset of the mAbs in epitope bin IV, which competitively bound to Nectin-2 with the mAbs in VII (Figure 4), also showed potent ADCC (data not shown). The epitope recognized by these antibodies is likely to be a critical spot for demonstrating potent ADCC.

As mentioned previously, I found 8 anti-Nectin-2 mAbs that showed inhibitory activities in the OV-90 cell proliferation assay. Interestingly, 7 out of them belonged to epitope bin VI (Figure 5) and the all 7 mAbs had a similar complementarity determining region (CDR) sequence (data not shown). The results suggest that I successfully screened a subset of anti-Nectin-2 mAbs that suppressed the proliferation of OV-90 cells even though their efficacies were not marked.

The anti-Nectin-2 mAbs, Y-443 representing epitope bin VII showed *in vivo* anti-tumor effects on OV-90 and MDA-MB-231 cells (Figures 9 and 10), and as discussed in Results, all the experimental results suggested that ADCC is the main mechanism of

action of Y-433. Thus, Nectin-2 was shown to be a promising target for antibody-based cancer therapies.

Tables and Figures

Table 1. Over-expression of Nectin-2 protein in breast and ovarian cancer tissues (IHC).

Breast cancer tissue	
Type	Positive rate
Infiltrating ductal carcinoma	16/18
Ductal carcinoma	7/7
Infiltrating lobular carcinoma	9/9
Medullary carcinoma	3/6
Mucinous adenocarcinoma	5/7
Paget's disease	7/7
	Positive/total

Ovarian cancer tissue	
Type	Positive rate
Serous carcinoma	22/40
Granular carcinoma	3/3
Clear cell carcinoma	1/2
Endometrioid	0/1
Mucinous carcinoma	1/4
Brenner tumor	1/1
Germinoma	0/4
Theca cell carcinoma	1/1
Metastasis carcinoma	1/6
	Positive/total

Table 2. Expression of Nectin-2 protein in normal tissues (IHC).

Tissue	Positive rate	Stained cells
Brain	0/3	
Breast	0/5	
Heart	0/3	
Lung	0/3	
Liver	3/3	Hepatocyte
Kidney	0/3	
Spleen	0/3	
Stomach	0/3	
Colon	0/3	
Rectum	0/3	
Ovary	0/3	
Prostate	0/3	
Testis	3/3	Spermatoblast

Figure 1. Over-expression of Nectin-2 mRNA in cancer tissues.

A box and whisker plot of the expression level of Nectin-2 mRNA in normal tissues and cancer tissues. Y axis represents Nectin-2 mRNA expression level. Nectin-2 mRNA expression in the indicated tissues was analyzed using Affymetrix U_133 arrays as described in Methods. The whiskers indicate the minimal and maximum values. The box indicates the 25th–75th percentile. N, normal tissues; C, cancer tissues. ***, $p < 0.0001$; **, $p < 0.01$; *, $p < 0.05$ as determined by the Mann Whitney test.

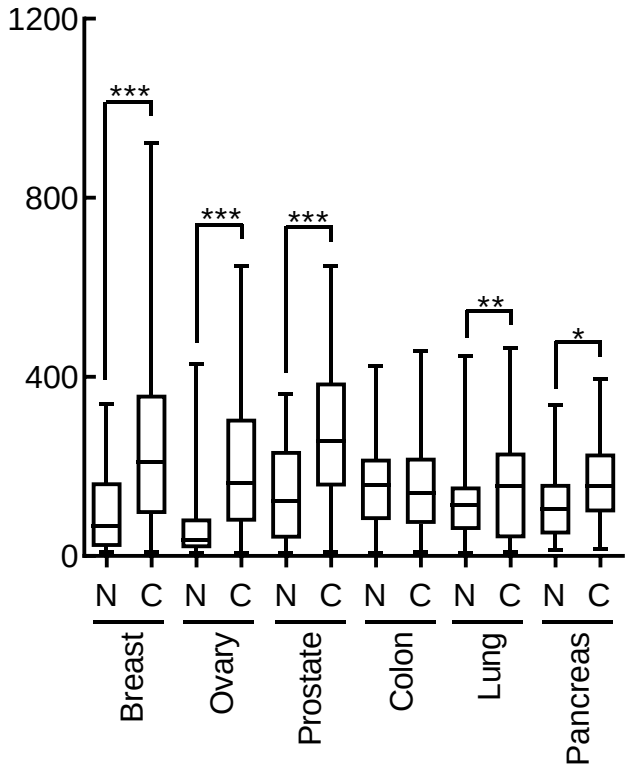
1200
800
400
0
***
***
***
**
*
N C N C N C N C N C N C
Breast
Ovary
Prostate
Colon
Lung
Pancreas

Figure 2. Over-expression of Nectin-2 protein in breast and ovarian cancer tissues. Paraffin-embedded tissue sections were stained with anti-Nectin-2 poAb as described in Methods. A, Normal breast tissue, B-D, breast infiltrating ductal carcinoma tissues. E, normal ovarian tissue, and F-H, ovarian serous carcinoma tissues.

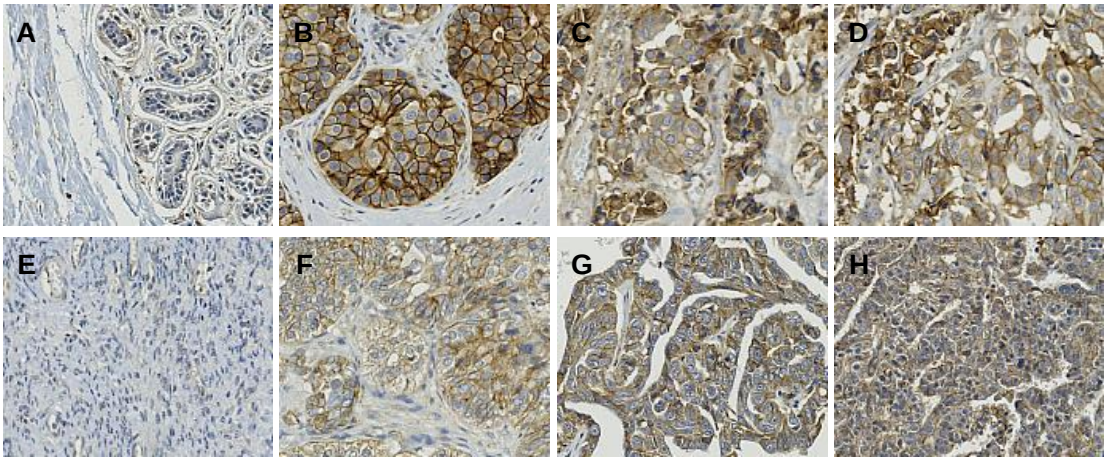
A
B
C
D
E
F
G
H

Figure 3. Over-expression of Nectin-2 in cancer cell lines.

Expression levels of Nectin-2 in various human cancer cell lines were examined by flow cytometry analysis using anti-Nectin-2 rabbit poAb.

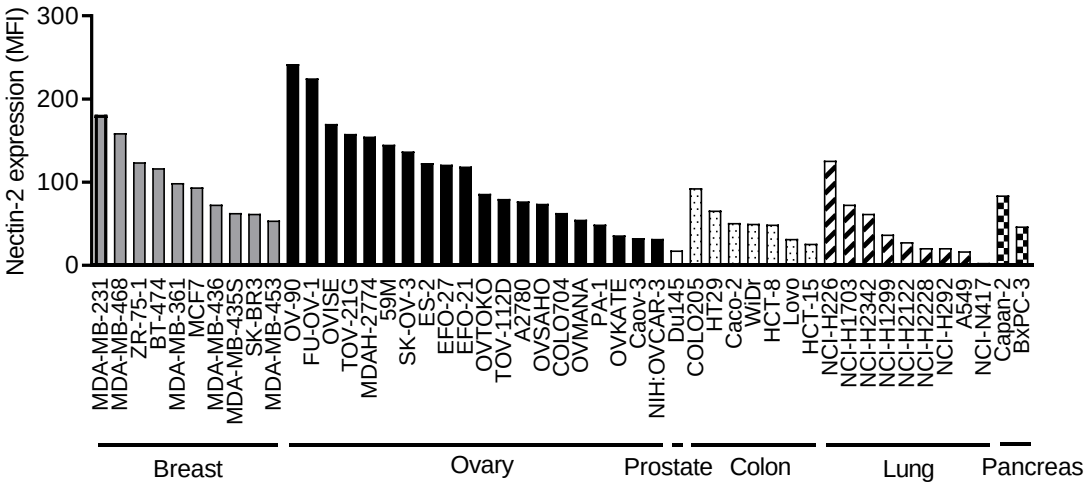
Nectin-2 expression (MFI)
300
200
100
0
MDA-MB-231
MDA-MB-468
ZR-75-1
BT-474
MDA-MB-361
MCF7
MDA-MB-436
MDA-MB-435S
SK-BR3
MDA-MB-453
OV-90
FU-OV-1
OVISE
TOV-21G
MDAH-2774
59M
SK-OV-3
ES-2
EFO-27
EFO-21
OVTOKO
TOV-112D
A2780
OVSAHO
COLO704
OVMANA
PA-1
OVKATE
Caov-3
NIH:OVCAR-3
Du145
COLO205
HT29
Caco-2
WiDr
HCT-8
Lovo
HCT-15
NCI-H226
NCI-H1703
NCI-H2342
NCI-H1299
NCI-H2122
NCI-H2228
NCI-H292
A549
NCI-N417
Capan-2
BxPC-3
Breast
Ovary
Prostate
Colon
Lung
Pancreas

Figure 4. Epitope binning of anti-Nectin-2 mAbs.

Each column and row in the matrix represents an unlabeled and biotinylated anti-Nectin-2 mAb, respectively. The red, yellow, and white cells show a combination of antibodies that showed > 70%, > 50%, and < 50% competitive binding inhibition, respectively. The dendrogram shown on the left side of the matrix was obtained by a cluster analysis using SpotFire DecisionSite for Lead Discovery.

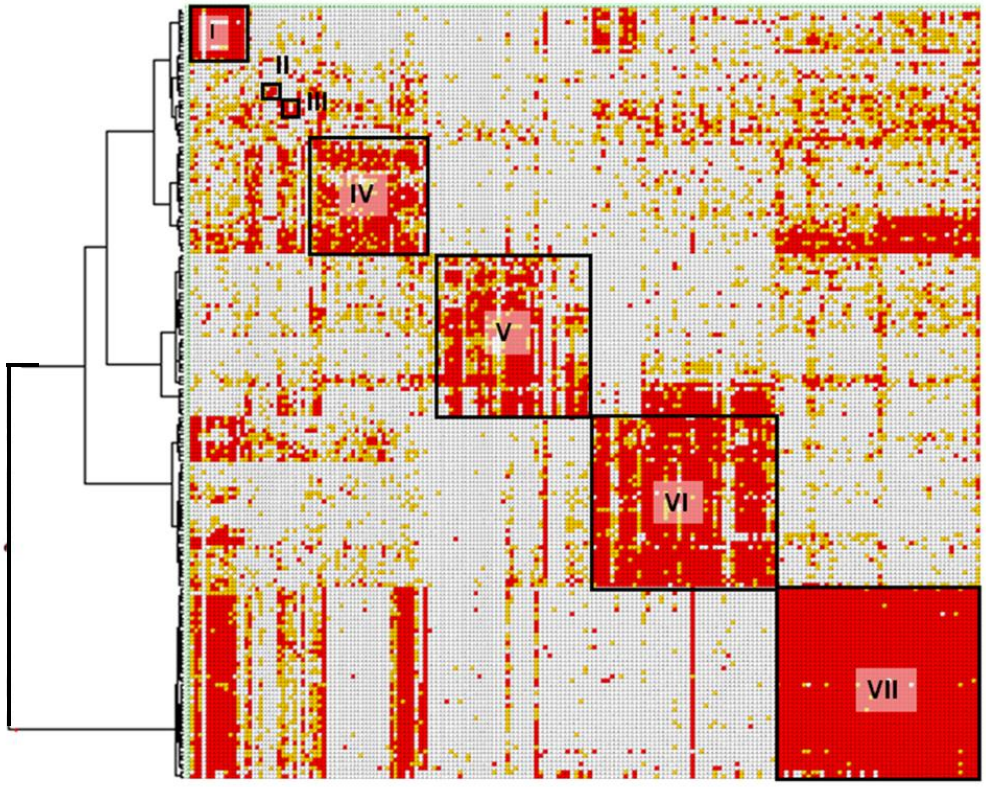
I
II
III
IV
V
VI
VII

Figure 5. Inhibitory activity of anti-Nectin-2 mAbs on the proliferation of OV-90 cells.

OV-90 cells were cultured in the presence of 30 μg/ml anti-Nectin-2 mAbs and poAb with 1% FBS for 6 days. The percentage inhibition of cell proliferation on the vertical axis is the mean ± S.D. of triplicate assays. *; antibodies that showed minus values for cell growth inhibition. #; antibodies that showed reproducible cell growth inhibition.

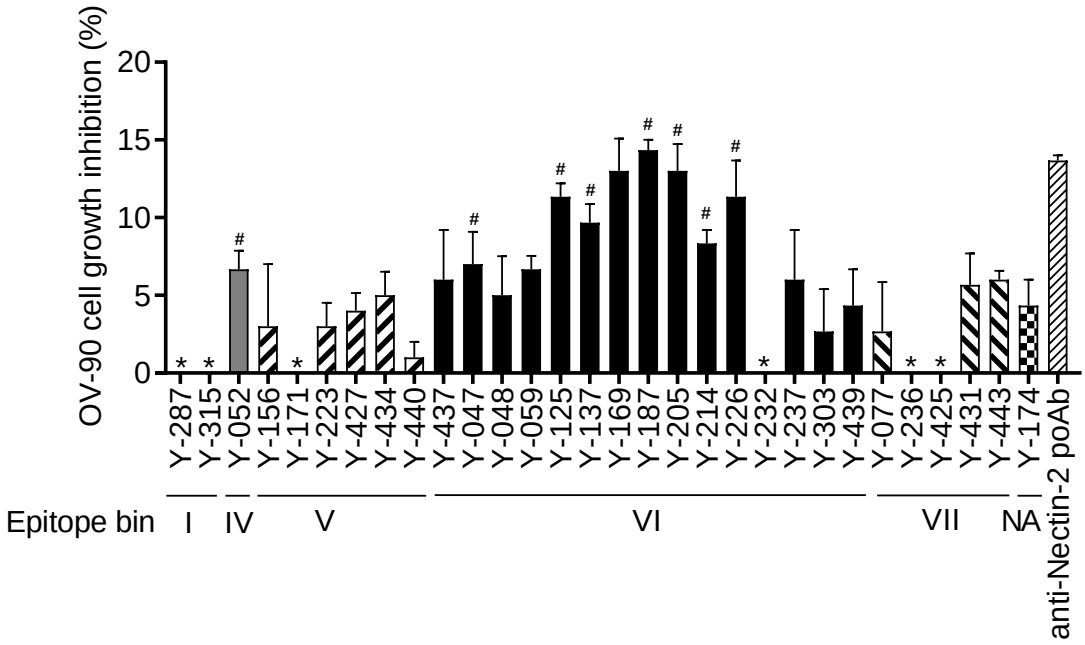
OV-90 cell growth inhibition (%)
20
15
10
5
0
Y-287
Y-315
Y-052
Y-156
Y-171
Y-223
Y-427
Y-434
Y-440
Y-437
Y-047
Y-048
Y-059
Y-125
Y-137
Y-169
Y-187
Y-205
Y-214
Y-226
Y-232
Y-237
Y-303
Y-439
Y-077
Y-236
Y-425
Y-431
Y-443
Y-174
anti-Nectin-2 poAb
Epitope bin
I
IV
V
VI
VII
NA

Figure 6. Inhibitory activity of anti-Nectin-2 mAb Y-187 on the proliferation of OV-90 cells.

OV-90 cells were cultured in the presence of the indicated concentrations of Y-178 (●), anti-Nectin-2 poAb (Δ) or control IgG (□) with 1% FBS for 6 days. The percentage inhibition of cell proliferation on the vertical axis is the mean ± S.D. of triplicate assays.

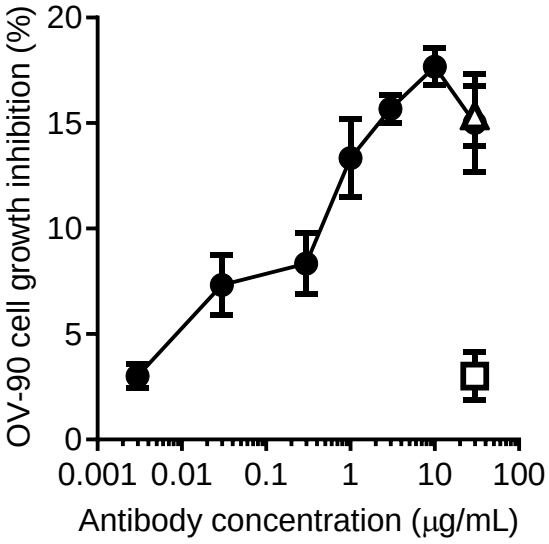
OV-90 cell growth inhibition (%)
20
15
10
5
0
0.001
0.01
0.1
1
10
100
Antibody concentration (μg/mL)

Figure 7. Inhibitory activity of anti-Nectin-2 mAbs on Nectin-2 *trans*-interaction.

Inhibitory activity of anti-Nectin-2 mAbs on Nectin-2-Nectin-3 *trans*-interaction (solid bar) and Nectin-2-Nectin-2 *trans*-interaction (blank bar) were measured by using an ELISA-based time-resolved fluorescence spectroscopy assay and a Biacore assay, respectively. The percentage inhibition of Nectin-2 *trans*-interaction on the vertical axis was calculated as described in Methods.

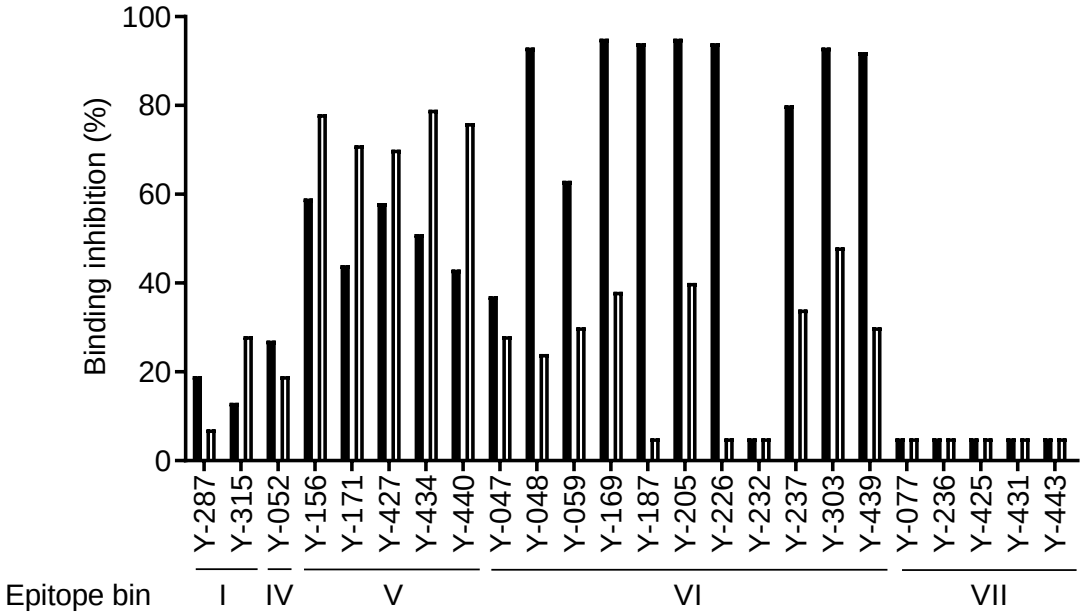
Binding inhibition (%)
100
80
60
40
20
0
Y-287
Y-315
Y-052
Y-156
Y-171
Y-427
Y-434
Y-440
Y-047
Y-048
Y-059
Y-169
Y-187
Y-205
Y-226
Y-232
Y-237
Y-303
Y-439
Y-077
Y-236
Y-425
Y-431
Y-443
Epitope bin
I
IV
V
VI
VII

Figure 8. ADCC of anti-Nectin-2 mAbs against OV-90 cells.

OV-90 cells pre-labeled with ^{51}Cr were incubated with anti-Nectin-2 mAbs and PBMC at an effector cell (PBMC): target cells (OV-90) ratio of 50:1 for 4 h at 37ºC, followed by the measurement of ^{51}Cr that was released into the culture supernatant. Specific cell lysis was calculated as described in Methods. The numbers in parentheses indicate the epitope bin of each antibody. The results are the mean ± S.D. of triplicate assays.

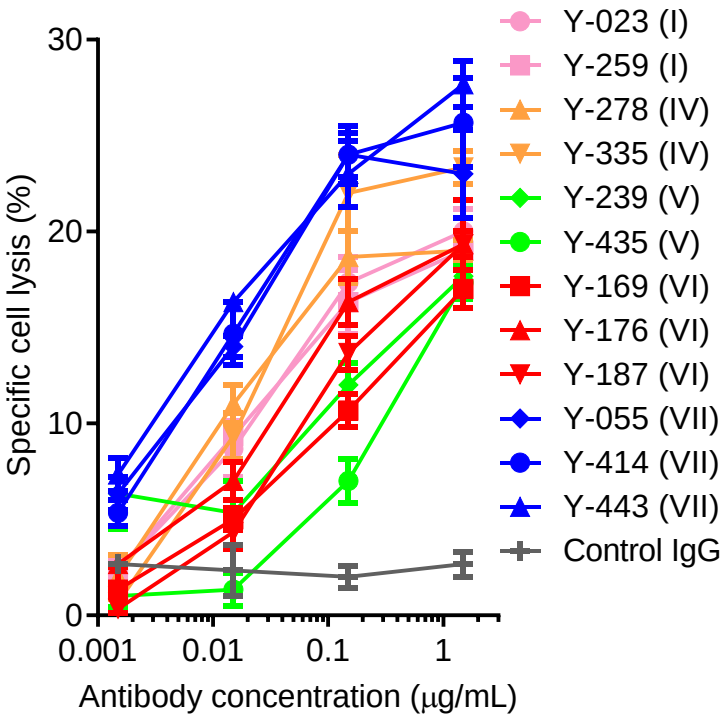
30
20
10
0
Specific cell lysis (%)
0.001
0.01
0.1
1
Antibody concentration (μg/mL)
Y-023 (I)
Y-259 (I)
Y-278 (IV)
Y-335 (IV)
Y-239 (V)
Y-435 (V)
Y-169 (VI)
Y-176 (VI)
Y-187 (VI)
Y-055 (VII)
Y-414 (VII)
Y-443 (VII)
Control IgG

Figure 9. *In vivo* anti-tumor effect of anti-Nectin-2 mAbs in the OV-90 mouse subcutaneous xenograft preventive model.

OV-90 cells were subcutaneously inoculated into the flanks of nude mice. On the same day, Y-187(□), Y-443 (▲) at a dose of 15 mg/kg or vehicle (●) was intravenously administered on a biweekly basis to the mice. The results are the mean ± S.D. **: $p < 0.001$ versus the vehicle group determined by Steel test.

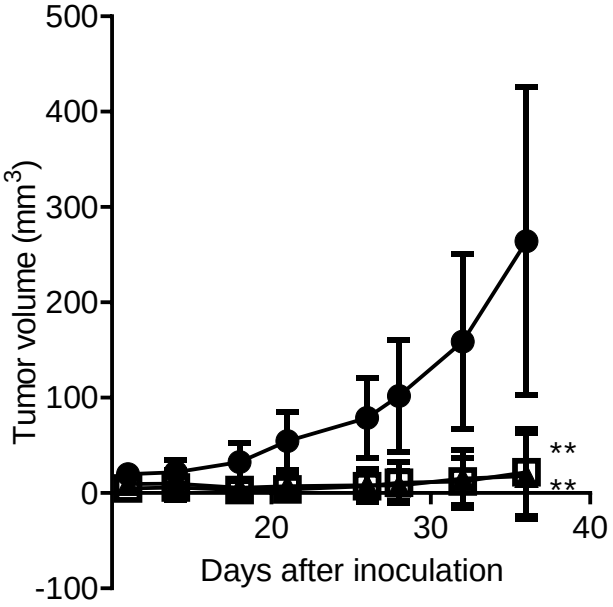
500
400
300
200
100
0
-100
Tumor volume (mm3)
20
30
40
Days after inoculation
**
**

Figure 10. *In vivo* anti-tumor effect of Y-443 in the established MDA-MB-231 mouse lung metastasis model.

MDA-MB-231 cells were intravenously injected into nude mice. From day 33, various doses of Y-443 or vehicle were intravenously administered on a weekly basis into the mice. The results are the mean ± S.D. at day 61. *: $p < 0.025$, versus vehicle group as determined by the one-tailed Shirley-Williams test.

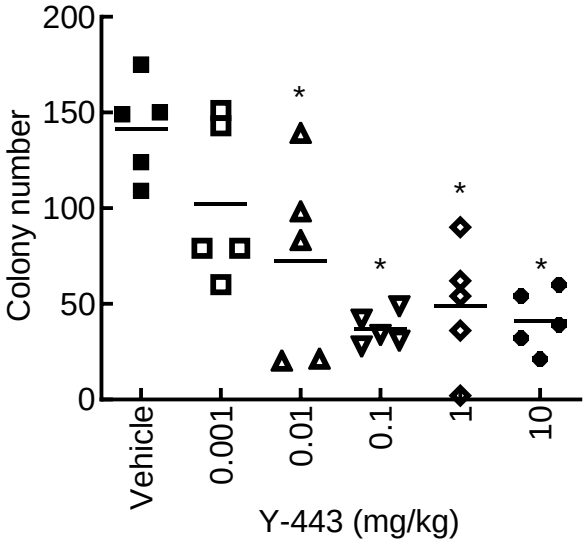
200
150
100
50
0
Colony number
*
*
*
Vehicle
0.001
0.01
0.1
1
10
Y-443 (mg/kg)

Figure 11. ADCC of Y-443 and its IgG_4 against MDA-MB-231 cells.

MDA-MB-231 cells pre-labeled with ^{51}Cr were incubated with Y-443 (●), Y-443 IgG_4 (▲), or control human IgG (□), and PBMC at an effector cell (PBMC): target cell (MDA-MB-231) ratio of 50:1 for 4 h at 37ºC, followed by measurement of ^{51}Cr that was released into the culture supernatant. Specific cell lysis was calculated as described in Methods. The results are the mean ± S.D. of triplicate assays.

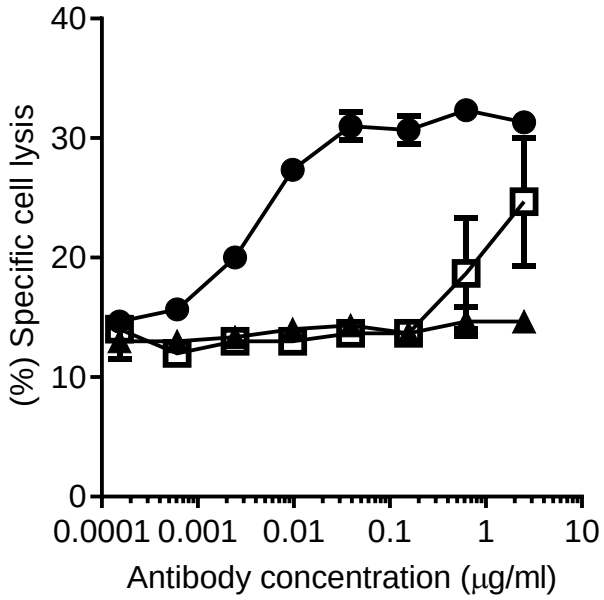
40
30
20
10
0
(%) Specific cell lysis
0.0001
0.001
0.01
0.1
1
10
Antibody concentration (μg/ml)

Figure 12. *In vivo* anti-tumor effect of Y-443 and its IgG_4 in the established MDA-MB-231 mouse subcutaneous xenograft model.

MDA-MB-231 cells were injected into SCID mice, and the mice were then treated with Y-443 IgG_1 (A) and Y-443 IgG_4 (B) on days 36, 43, and 50 after cell injection ($n = 5$). The results are the mean ± S.D. *: $p < 0.025$ versus the control as determined by the one-tailed Williams test.

A Y-443 IgG_1

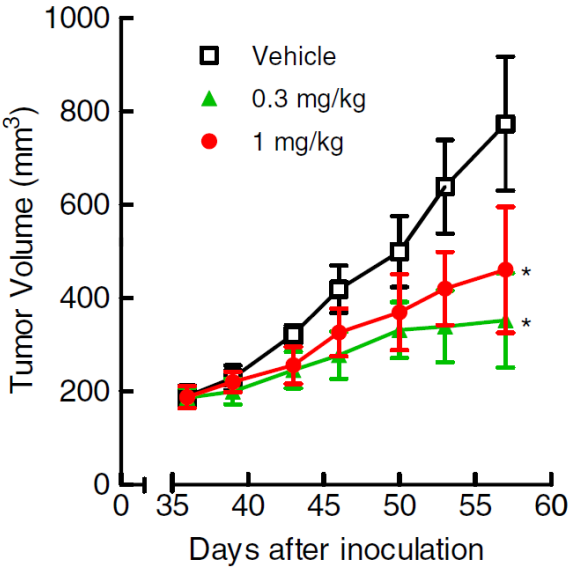

B Y-443 IgG_4

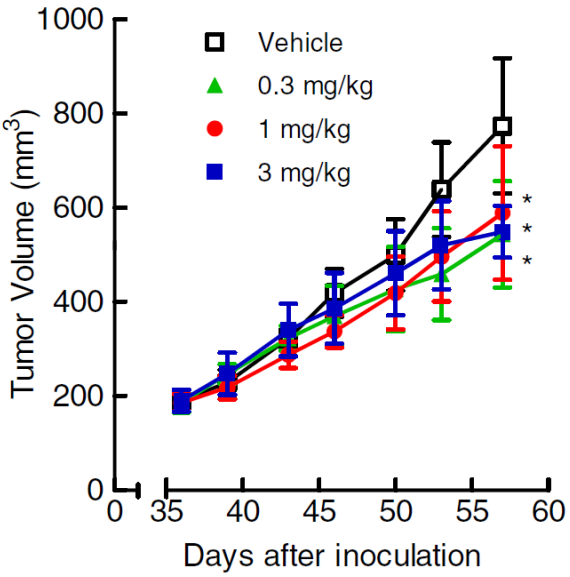

Figure 13. CDC of Y-443 against MDA-MB-231 cells.

MDA-MB-231 cells and Daudi cells were incubated with Y-443 or rituximab together with human serum complement for 60 min at 37ºC, respectively. The damaged cells were stained with propidium iodide. Antibody-specific CDC was calculated as described in Methods. The results are the mean ± S.D. of triplicate assay.

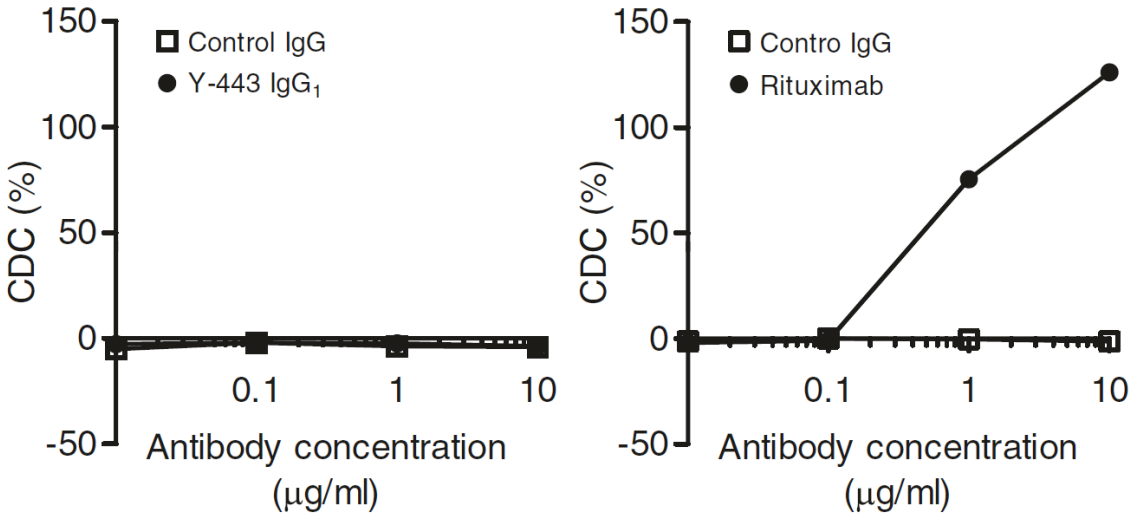
150
100
50
0
-50
CDC (%)
Control IgG
Y-443 IgG1
0.1
1
10
Antibody concentration
(μg/ml)
150
100
50
0
-50
CDC (%)
Contro IgG
Rituximab
0.1
1
10
Antibody concentration
(μg/ml)

Chapter 2:

Fc Engineering of Anti-Nectin-2 Antibody Improved Thrombocytopenic Adverse Event in Monkey

Abstract

In chapter 1, I have demonstrated that Nectin-2 is over-expressed in breast and ovarian cancer tissues by using gene expression analysis and immunohistochemistry. Furthermore, I discovered multiple anti-Nectin-2 fully human monoclonal antibodies which inhibited tumor growth in *in vivo* subcutaneous xenograft models with antibody-dependent cellular cytotoxicity (ADCC) as the principal mechanism of action. In the studies described in this chapter, I assessed the toxicity of Y-443, a fully human IgG_1/kappa anti-Nectin-2 monoclonal antibody exhibiting strong *in vitro* ADCC and *in vivo* anti-tumor activity in cynomolgus monkeys (*Macaca fascicularis* (Cynos)). Unexpectedly, upon administration, Y-443 induced strong thrombocytopenia through Nectin-2 expressed on Cyno platelets, presumably followed by phagocytosis in the mononuclear phagocytic system. To mitigate the adverse safety profile, I mutated the Fc region of Y-443 to reduce the Fc binding activity to Fcγ receptor I, which is the primary receptor for phagocytosis on macrophages. Moreover, I further engineered the Fc through defucosylation to maintain ADCC activity. The resultant Fc engineered antibody, termed Y-634, demonstrated diminished thrombocytopenia in Cyno toxicological studies and maintained anti-tumor activity in a mouse xenograft model. These findings suggest that Y-634 may have a therapeutic potential for the treatment of Nectin-2 positive cancers, and moreover, Fc engineering is a potential mitigation strategy to ameliorate safety liabilities in antibody induced thrombocytopenia while maintaining antibody potency.

Introduction

Nectin-2, a single-pass type I transmembrane glycoprotein with an extracellular region consisting of three immunoglobulin (Ig) -like domains, is a plasma membrane component of adherens junctions that mediates Ca^{2+}-independent cell-cell adhesion (Takai et al., 2003). Previous studies reported that the second Ig-like domain is important for the formation of Nectin-2-Nectin-2 homo-*cis*-dimers (Lopez et al., 1998; Satoh-Horikawa et al., 2000; Miyahara et al., 2000; Reymond et al., 2001; Febre et al., 2002; Momose et al., 2002; Takai et al., 2003; Yasumi et al., 2003). The Nectin-2 homo-*cis*-dimer is able to interact with other Nectin-2 homo-*cis*-dimer or Nectin-3 homo-*cis*-dimer expressed on other cells to form homo-*trans*-dimers or hetero-*trans*-dimers, respectively, via the first Ig-like domain in Nectin-2 or Nectin-3 (Lopez et al., 1998; Satoh-Horikawa et al., 2000; Miyahara et al., 2000; Reymond et al., 2001; Febre et al., 2002; Momose et al., 2002; Takai et al., 2003; Yasumi et al., 2003). Those homo- and hetero-*trans*-dimers then induce other cell-cell adhesion event via other cell adhesion molecules such as E-cadherin and claudin, to form tight junction (Fukuhara et al., 2002a; Fukuhara et al., 2002b; Fukuhara et al., 2003; Morita et al., 2010). Nectin-2 also plays a role as organizer of Sertoli cell-spermatid junctions and synapse formation in testes and neurons, respectively (Bouchard et al., 2000; Mizogushi et al., 2002; Inagaki et al., 2003). Furthermore, in addition of cell adhesion functions, Nectin-2 mediates both entry and spreading of infection from various viruses (Warner et al., 1998) and has also been reported that DNAM-1 (CD226) and TIGIT interact Nectin-2 to activate immune cells (Bottino et al., 2003; Tahara-Hanaoka et al., 2004; Stanietsky et al., 2009; Chan et al., 2012).

In a previous study (chapter 1), I reported that Nectin-2 is over-expressed in breast and ovarian cancer and is involved in cancer proliferation. I generated numerous Nectin-2-specific fully human monoclonal antibodies (mAbs) and demonstrated the anti-tumor effect of the selected mAb clone, Y-443 (human IgG_1/kappa), on breast cancer and ovarian cancer cells. I also performed *in vitro* and *in vivo* studies of Y-443 and Y-443 IgG_4 (where the constant region is substituted to human IgG_4 isotype) and found that the main mechanism of action appeared to be antibody-dependent cellular cytotoxicity (ADCC).

The toxicological studies have been conducted in cynomolgus monkeys (*Macaca fascicularis* (Cynos)) since Y-443 did not cross-react to mouse Nectin-2, but cross-reacted Cyno Nectin-2 with affinity nearly identical to human Nectin-2. While the anti-tumor effect was promising, the anti-Nectin-2 mAb exhibited unexpected "idiopathic thrombocytopenic purpura (ITP)-like" thrombocytopenia in Cynos. ITP is an immune-mediated bleeding disease chiefly caused by autoantibodies directed against membrane-bound targets including GPIIb/IIIa and GPIb-IX on platelets (McMillan et al., 1987; Semple et al., 1995; Coopamah et al., 2003), resulting in phagocytosis in the mononuclear phagocytic system (MPS). Conversely, it has been reported that other platelet antigens can cause thrombocytopenia via alternative mechanism of actions (Webster et al., 2006; Go et al., 2007). In addition to autoantibodies, it has also been reported that therapeutic antibodies such as anti-TNFα (infliximab), anti-CD11a (efalizumab), and anti-CD20 (rituximab) antibodies occasionally trigger platelet-specific autoantibodies and induce thrombocytopenia; however the mechanism of action remained unclear (Everds et al., 2013). Previous reports have shown that the clearance of platelets coated with IgG autoantibodies is accelerated by phagocytosis through Fcγ

receptors (FcγRs) expressed on tissue macrophages in the reticuloendothelial system, particularly in the spleen (Semple et al., 1995; Cines et al., 2002; Coopamah et al., 2003). Wallace et al. suggested that FcγRI is the most relevant to phagocytosis of antibody-bound platelets by macrophages (Wallace et al., 1997), and intravenous infusion of gammaglobulin (IVIg) and Fcγ fragments has been used clinically for the treatment of such ITP to prevent the phagocytic events (Debre et al., 1993; Bussel et al., 2000).

Therapeutic antibodies are predominantly comprised of human IgG_1 and can elicit immune effector functions via the engagement of both humoral and cell-mediated immunity through interaction with the Fc portion of the antibody. It has been reported that Leu234-Gly237 of human IgG_1, particularly Leu235 is a critical amino acid for mediating the Fc-FcγRI interaction (Duncan et al., 1988; Jefferis et al., 1990; Chappel et al., 1991; Lund et al., 1991; Morgan et al., 1995; Desjarlais et al., 2007). In this chapter, I report that the anti-Nectin-2 antibody Y-443 induces strong thrombocytopenia in Cynos. I further present the ability of Fc engineering, including Leu235-substitution and defucosylation of Y-443, to ameliorate thrombocytopenia through decreased binding to FcγRI while presenting ADCC that is essential for its pharmacological activity.

Materials and Methods

Cells

MDA-MB-231 cells were purchased from the American Type Culture Collection. MDA-MB-231 cells were grown in Leibovitz's L-15 medium containing 10% fetal bovine serum in a humidified incubator at 37°C.

Preparation of Recombinant Proteins

Recombinant extracellular domains (ED) of human or Cyno Nectin-2 fused with FLAG (Nectin-2-ED-FLAG) or human Fc (Nectin-2-ED-Fc) at its C-terminus were prepared as described previously in Chapter 1. Recombinant human FcγRI and FcγRIIa were purchased from R&D systems. Recombinant human FcγRIIb and FcγRIIIa (158F) were prepared in-house. Briefly, a eukaryotic expression vector pcDNA3.1 in which a cDNA encoding a sequence of extracellular domain of FcγR with a 6 histidine-tag at its C-terminus was inserted was constructed, and it was transiently expressed in FreeStyle 293-F cells by FreeStyleTM 293 Expression System (Invitrogen). The recombinant proteins were purified from the culture supernatant by Ni-NTA Agarose affinity chromatography.

Production and Fc Modification of Anti-Nectin-2 mAbs

Anti-Nectin-2 fully human mAb, Y-443, was generated by immunizing transchromosomic fully human antibody producing mice carrying the complete locus for the human immunoglobulin heavy chain gene and a transgene for the human immunoglobulin kappa light chain (Kyowa Hakko Kirin Co., Ltd.) with recombinant

Nectin-2 protein as described in Chapter 1. The cDNAs encoding the variable regions of heavy chain and light chain of the antibody were isolated from the hybridoma, and were inserted into the GS expression vector pEE6.4 (Lonza Biologics) with human IgG_1 constant region and pEE12.4 (Lonza Biologics) with human kappa constant region, respectively. The two vectors were combined to obtain a double-gene vector carrying the heavy and light chain according to the manufacturer's guidelines. The expression vector was transfected into CHOK1SV cells, and a stable transfectant was obtained according to manufacturer's standard protocols. The stable transfectant was expanded in CD CHO medium (Invitrogen) containing 25 mM methionine sulfoximine, and the recombinant Y-443 antibody was purified from the culture supernatant by recombinant protein A chromatography (MabSelect SuRe, GE Healthcare), followed by ion-exchange chromatography using Capto Q and Capto S columns (GE Healthcare). The purified Y-443 was concentrated and buffer-exchanged in Dulbecco’s phosphate buffered saline. Endotoxin removal was performed using ActiClean Etox resin (Sterogene Bioseparations) according to manufactures guidelines.

To generate Fc mutants, a single amino acid mutation to aspartic acid (Asp, D) or tyrosine (Tyr, Y) was introduced at leucine (Leu, L) position 235 (Kabat numbering) in the heavy chain gene of Y-443 using QuikChange Lightning Site-Directed Mutagenesis Kit (Stratagene) with corresponding primers and the double gene vector encoding Y-443 as a template. The Fc mutant vectors were transiently transfected to FreeStyle 293-F cells using the FreeStyleTM 293 Expression System. The recombinant Fc variant antibodies were purified from the culture supernatant by Protein A chromatography, followed by size-exclusion chromatography and membrane filtration.

The recombinant defucosylated Y-443 (L235D) antibody, termed Y-634, was prepared by transfection of Y-443 (L235D) plasmid into fucosyltransferase knockout CHO cells (POTELLIGENT® Cells, BioWa, Inc.) and stable transfectants were generated. One of the stable transfectants, #90-4, was further cultured in 90% CD CHO, 10% CD DG44 (Invitrogen) medium, and the expressed Y-634 was purified from the culture supernatant as described in aforementioned methods.

Analysis of Recombinant Anti-Nectin-2 mAbs

The purity of the recombinant antibodies was tested by SDS-PAGE and a size-exclusion chromatography using Superdex 200 10/300 GL (GE Healthcare). Endotoxin content was measured by Endospecy ES-24S Set (Seikagaku Co.). L-fucose content of the antibodies was determined by the carbohydrate constituent analysis (Kurokawa et al., 2002).

Binding Activity of Anti-Nectin-2 mAbs to Human and Cyno Nectin-2 or Human FcγRs

Antigen binding affinity of the anti-Nectin-2 mAbs was evaluated by a kinetic measurement with a BIACORE 2000 using recombinant human and Cyno Nectin-2-ED-Fc proteins, and the equilibrium dissociation constant (K_D) was determined using BIAevaluation software. The binding of Y-443 and the Fc engineered antibodies against human FcγRs was measured by an ELISA using immunoplates coated with recombinant human FcγRI, FcγRIIa, FcγRIIb, and FcγRIIIa (158F). Various concentrations of antibodies were applied to the plates, and the bound antibody was detected by HRP-labeled anti-human IgG (H+L) antibody (Immuno-Biological Labolatories Co., Ltd). The EC_{50} was determined by GraphPad Prism (GraphPad Software, Inc.).

Pharmacological Studies in Mice

The anti-tumor effect of anti-Nectin-2 mAbs was evaluated in a mouse subcutaneous xenograft model. C.B17/Icr-scid/scid Jcl mice (6-week old, female) were purchased from CLEA Japan. Mice were housed in groups of 5 per plastic cage and were acclimated for at least 7 days prior to study start. Room temperature was maintained at 24±1°C with a 12/12 hour light/dark cycle. Food and water were available ad libitum. A 100 µL volume of MDA-MB-231 breast cancer cells (3×10^6 cells) and Matrigel (Becton Dickinson) was subcutaneously inoculated into the left flank of mice. When the tumor volume reached to around 120 - 200 mm^3, the mice were randomly grouped. In the first experiment, dose escalating Y-443 (0.1, 0.3, 1, 3 and 10 mg/kg/10 mL) and vehicle (Dulbecco's phosphate buffered saline (-)) were intravenously injected to 5 mice in each treatment group once a week for 3 weeks under physical restraint. Tumor diameter was measured with a calliper twice per week and the approximate tumor volume was calculated by the equation of $0.5 \times \text{length} \times (\text{width})^2$ during the treatment period to monitor tumor growth. In the second experiment, the anti-tumor effect of Y-634 (0.1, 0.3, and 1 mg/kg/10 mL) was compared to that of Y-443 (0.3 mg/kg/10 mL) using the methodology described in the first experimental group. Statistical analysis was performed by the Williams' test.

Housing of Cynos

All of Cynos (*Macaca fascicularis* at 3 years and 2 months to 5 years and 8 months of age, Nafovanny and/or Siconbrec) were individually housed in metal cages set on racks in an animal room based on the protocol of toxicological study approved by

the Committee on the Ethics of Animal Experiments of Takeda Pharmaceutical Company Limited. Each monkey was fed 150 g of a pelleted diet (Certified primate diet #5048, PMI Feeds Inc.) once-daily. The Cynos were allowed free access to tap water.

Toxicological Studies in Cynos

Single dose of Y-443 (1, 3, 10, and 50 mg/kg) and vehicle (25 mM sodium acetate, 125 mM NaCl [pH 5.5]) were intravenously injected (2 mL/minute) to 2 male and 2 female monkeys (Nafovanny and Siconbrec) in each group followed by 2 weeks observation period. Single dose of Y-634 (10 mg/kg) was also intravenously injected to 2 male monkeys (Siconbrec) followed by 2-week observation period. Y-634 (3 and 10 mg/kg/week) and vehicle (Dulbecco's phosphate buffered saline (-)) were intravenously injected for 3 weeks to 2 female monkeys (Nafovanny and Siconbrec) in each group followed by 2-week observation period. Clinical signs, body weights, food consumption, bleeding time, hematology, coagulation test, gross pathology, organ weights, histopathology and/or toxicokinetics were examined. Blood samples for hematology were collected from femoral vein of each animal using a syringe with sodium heparin and were transferred to tubes containing EDTA-2K under physical restraint. Blood samples for coagulation test were collected from femoral vein with a syringe containing 0.1 mL of 3.13% sodium citrate and were centrifuged at 1500×g for 10 minutes to obtain plasma. The values of hematology were determined or calculated with an automated hematology analyzer (ADVIA120, Siemens Healthcare Diagnostics K.K.) and the values for coagulation test were determined with an automated blood coagulation analyzer (CA-1000, Sysmex Corporation). F gross pathology, organ weights and histopathology, all of Cynos were anesthetized by intramuscular injection of

ketamine hydrochloride and were euthanized by exsanguinations from the common carotid artery at necropsy. Systemic organs for histopathology were fixed in 10 volume percent (vol. %) neutral buffered formalin. The eyes and testes were fixed in 2.5 weight/volume percent glutaraldehyde in 10 vol. % neutral buffered formalin and Bouin's fluid, respectively, and then preserved in 10 vol. % neutral buffered formalin. Fixed samples were embedded in paraffin, sectioned, stained with hematoxylin and eosin, and examined microscopically. Blood samples for toxicokinetics were collected from the vein of the extremities by syringes and transferred to tubes containing separating agent and were centrifuged at about 1500×g for 15 minutes to obtain plasma and stored in ice.

Measurement of Y-443 or Y-634 in Cyno Serum

Cyno serum samples were applied to immunoplates coated with recombinant human Nectin-2 protein (R&D systems). The bound antibody was detected by HRP-labeled anti-human IgG (H+L) antibody (Immuno-Biological Labolatories Co., Ltd). The serum concentration of Y-443 or Y-634 was calculated from its standard curve.

ADCC Assay

Human peripheral blood mononuclear cells (PBMC) purchased from AllCells, LLC and were cultured in RPMI1640 medium containing 10% fetal bovine serum, 0.1 nM human IL-2 (DIACLONE Research) and 55 μM 2-mercaptoethanol for 24 hours. PBMC were incubated with Calcein AM-labeled MDA-MB-231 cells at a ratio of 50:1 in the presence of anti-Nectin-2 mAb for 4 hours at 37ºC. After the incubation, total and

dead MDA-MB-231 cell numbers were measured and dead cell ratio was calculated by Acumen Explorer (TTP labtech).

Ethics Statement

All of the animal studies were carried out in strict accordance with the recommendations in the Guide for the Care and Use of Laboratory Animals of the National Institutes of Health. The protocols were approved by the Committee on the Ethics of Animal Experiments of Takeda Pharmaceutical Company Ltd. (Permit Numbers for Cyno studies: TEACUC-A1-012 and TEACUC-A1-014, Permit Number for mouse studies: TEACUC-E1-031).

Results

Tumor growth inhibition by Y-443 against MDA-MB-231 in a mouse subcutaneous xenograft model

As shown in the chapter 1, Y-443, one of the anti-Nectin-2 fully human mAbs, significantly inhibited tumor growth in a MDA-MB-231 mouse subcutaneous xenograft model with ADCC as the central mechanism of action. Here, I evaluated Y-443 in the same MDA-MB-231 mouse subcutaneous xenograft model with lower dose to determine its minimum effective dose. As shown in Figure 14, Y-443 significantly demonstrated potent anti-tumor effect at 0.3 mg/kg, but not at 0.1 mg/kg.

Adverse effects of Y-443 in Cynos

As described above, Y-443 demonstrated an *in vivo* anti-cancer effect suggesting the potential for a therapeutic anti-cancer antibody. Unfortunately, the Y-443 did not cross-react to mouse Nectin-2-ED-Fc; however, Y-443 cross-reacts to Cyno Nectin-2-ED-Fc with a nearly identical affinity to human Nectin-2-ED-Fc (K_D = 5.8 nM vs. 4.9 nM, determined by kinetic analysis with Biacore). Therefore, toxicological studies were carried out in Cynos. Single intravenous bolus injection of Y-443 at 10 mg/kg or 50 mg/kg (2 males and 2 females in each group) did not cause death or treatment-related abnormalities as measured by clinical signs including body weights and food consumption for 2 weeks over the observation period. However, in the hematological examination, a decrease in platelet count was observed on days 1 and 7 in nearly all animals dosed at 10 mg/kg. Recovery of the platelet counts was observed on day 14 in all monkeys with the exception of one male monkey (Table 3 and Figure 15).

At the higher 50 mg/kg dosage, the thrombocytopenia continued for 2 weeks post dosing. The platelet count decreased to less than $10 \times 10^4/\mu L$ in almost all animals dosed at 10 and 50 mg/kg ranging from 2 to 42% of pre-treatment values. Decreases in erythrocyte count, hematocrit value and hemoglobin concentration were also observed on days 7 and 14 in one male and all females dosed with 50 mg/kg Y-443. Additionally, the reticulocyte count was found to be increased on days 7 and 14 in most animals dosed with 10 and 50 mg/kg (Table 3), but no changes in leukocytes numbers were observed (data not shown). On day 15, prolongation of bleeding time was observed in 1 male dosed of 10 mg/kg and the both males and one female dosed of 50 mg/kg (Table 4). These changes were considered to be secondary events to thrombocytopenia. Conversely, no treatment-related abnormality was observed in coagulation tests, including prothrombin time (PT), activated partial thromboplastin time (APTT) and plasma fibrinogen in any of the monkeys (Table 4).

All Cynos were sacrificed 2 weeks post dosing and subjected to necropsy and histopathological examination. Hemorrhage was observed in several organs (liver, heart, lung, stomach, testis, pancreas, lymph nodes, thymus, thyroids, adipose tissue in abdominal cavity and skeletal muscle) for all of the Cynos dosed of 50 mg/kg. Increased spleen weight was observed in 1 male and 1 female dosed of 10 mg/kg and all the Cynos dosed of 50 mg/kg (Table 4). There were no perceived gender-differences in the aforementioned adverse events. All the symptoms observed in Y-443-treated Cynos, including thrombocytopenia, bleeding tendency, hemorrhage in various organs and splenomegaly, were similar to typical symptom of ITP.

In order to investigate the dose-dependency of the thrombocytopenia, I included two additional experimental groups, each consisting of two male monkeys

treated with bolus injections of either 1 or 3 mg/kg Y-443. Marked decreases in platelet count were reproduced on day 1 in both administration groups (Figure 15). The platelet count recovered earlier in 1 mg/kg group compared to the higher dose groups, although, dose-dependency between 3 and 10 mg/kg groups was insignificant. In toxicokinetics studies, Cynos administered with lower doses of Y-443, especially in the 1 and 3 mg/kg groups, showed accelerated serum clearance of the antibody (Figure 16). Collectively, the results suggest the severity of thrombocytopenia is dependent on the serum concentration of Y-443.

Fc engineering to mitigate thrombocytopenia

Multiple studies revealed that ITP is triggered by binding of autoantibodies against self-antigens on platelets, and the interaction of the IgG Fc with FcγRI on macrophages drives phagocytosis in the spleen (McMillan et al., 1987; Semple et al., 1995; Bussel et al., 2000; Coopamah et al., 2003). As such, I speculated the possibility of mitigating the Y-443-induced thrombocytopenia through modulating the interaction between the Fc region of antibody and FcγRI. Fortunately, multiple previous studies revealed that mutations of Leu235 (Kabat numbering) was capable of weakening the Fc-FcγRI interaction (Duncan et al., 1988; Jefferis et al., 1990; Chappel et al., 1991; Lund et al., 1991; Morgan et al., 1995; Desjarlais et al., 2007). Hence, I generated several Fc mutants of Y-443 and evaluated their binding to recombinant human FcγRs in an ELISA based assay. Furthermore, I also measured the equilibrium dissociation constant (K_D) against human Nectin-2 by BIACORE to confirm retained target binding activity of the Fc mutant antibodies. I identified two mutants, Y-443 (L235Y) and Y-443 (L235D), both of which exhibited a significant decrease in binding to FcγRI, but retained antigen

binding activity relative to the Y-443 parental antibody (Table 5). The Y-443 (L235Y) mutant also exhibited moderate decrease in binding to FcγRIIa and FcγRIIb, and 30-fold reduction in binding to FcγRIIIa (158F). Alternatively, the Y-443 (L235D) mutant displayed a lesser change in binding to FcγRIIa and FcγRIIb, but only a 5-fold reduction in binding to FcγRIIIa was observed. Therefore, the Y-443 (L235D) mutant was selected for future studies as it demonstrated the most desirable features.

In consideration that ADCC is the primary mechanism for anti-tumor effect of Y-443 as demonstrated in the chapter 1, the ADCC of the Y-443 mutants was evaluated. As predicted by the decreased affinity to FcγRIIIa, ADCC of Y-443 (L235D) against MDA-MB-231 breast cancer cells was 10-fold lower than its parent antibody, Y-443 (Figure 17).

To rescue the decreased ADCC potency, I prepared a defucosylated variant of the Y-443 (L235D) mutant. Removal of the L-fucose from N-glycan linked to asparagine (Asn) residue at Kabat position 297 was accomplished by stably expressing a plasmid encoding Y-443 (L235D) antibody gene in POTELLIGENT® Cells. The recombinant defucosylated Y-443 (L235D) antibody, termed Y-634, was purified from the culture supernatant as described in Materials and Methods. The L-fucose content of Y-634-derived N-glycan was undetectable compared to those of Y-443 and Y-443 (L235D). The Nectin-2 binding affinity of Y-634 was identical to Y-443 and Y-443 (L235D) (Table 5). Moreover, the ADCC potency of Y-634 was comparable to Y-443 (Figure 17). Thus, I demonstrate successful development of Y-634, a defucosylated Y-443 (L235D) mutant, with significantly reduced binding to FcγRI while maintaining both Nectin-2 binding activity and ADCC.

Toxicological studies of Y-634 in Cynos

To investigate the pharmacovigilance, Y-634 was subjected to toxicological studies in Cynos. The effect of a single intravenous bolus injection (10 mg/kg) of Y-634 on plasma platelets was investigated in female monkeys (n = 2). Unfortunately, platelet counts were decreased to 30 × 10^4 and 41 × 10^4/μL level on day 1, although, there were no major changes in hematological values (Table 6). Nevertheless, the degree of thrombocytopenia was milder than those of Y-443, and the platelet level was maintained between 29 × 10^4 and 49 × 10^4/μL over the two-week observation period. The platelet levels never reached below 10 × 10^4/μL (or one third of the normal Cyno's platelet value), which for comparison, is assumed to be a critical level in human thrombocytopenia patients for observed prolonged bleeding time in terms of safety (CTCAE v3.0; https://ctep.cancer.gov/protocoldevelopment/electronic_applications/ctc.htm) (Figure 18 and Table 6). In a repeated intravenous administration study in Cynos, dosed at either 3 mg/kg/week or 10 mg/kg/week (n = 2), platelet counts were maintained above 22 × 10^4/μL for 4 weeks after the 1st dosing of Y-634 in the both groups and further reduction by repeated dosing was not observed. Necropsy or histopathological examination showed no notable changes which had been observed in the study of Y-443 (data not shown). Ultimately, the severe thrombocytopenia induced by Y-443 was markedly reduced through Fc engineering; however, complete elimination of thrombocytopenia was not observed.

Tumor growth inhibition by Y-634 against MDA-MB-231 in a mouse subcutaneous xenograft model

Y-634 showed similar ADCC activity compared to the parent antibody, Y-443, and demonstrated partially alleviated thrombocytopenia in Cynos (Figure 17). In the final experiment, I evaluated the anti-tumor effect of Y-634 in a mouse subcutaneous xenograft model of MDA-MB-231 breast cancer cells. Weekly administrations of Y-634 showed significant anti-tumor effect at 0.1 mg/kg and equivalent efficacy to Y-443 at 0.3 mg/kg (Figure 19). Altogether, these results suggest that Y-634 retains strong anti-tumor effect with significantly reduced thrombocytopenia.

Discussion

In chapter 1, I demonstrated that Nectin-2 is over-expressed in both breast and ovarian cancers. I subsequently developed an anti-Nectin-2 fully human mAb, Y-443, which has an *in vivo* anti-tumor effect on OV-90 and MDA-MB-231 xenograft models through an ADCC mechanism. Since the Y-443 cross-reacted to Cyno Nectin-2 with equivalent K_D to human Nectin-2 (4.9 nM and 5.8 nM, respectively), I conducted toxicological studies in Cynos. In a single dose study, intravenous administration of Y-443 (10 and 50 mg/kg) caused severe thrombocytopenia with prolonged bleeding time in all the animals (Table 3, Table 4, and Figure 15), despite that clinical signs and other hematological remained normal. Interestingly, the Nectin-2 expression was observed only in liver and testes (Figure 2), with negligible expression on human platelets (data not shown), hence, the adverse events observed in Cynos were unexpected. Here, Y-443 marginally detected Nectin-2 on Cyno platelets (data not shown), and furthermore, did not induce aggregation of monkey platelets at 100 μg/mL in *in vitro* (data not shown). Moreover, single intravenous administration of Y-443 at 10 and 50 mg/kg gave no meaningful changes in Cyno coagulation test (Table 3). The splenomegaly observed in those monkeys correlated to the activated phagocytic function of the spleen, which seemed to cause disposal of platelet-Y-443 complex resulting in thrombocytopenia and faster serum clearance of the antibody in the lower dose groups. The activated phagocytic function could conceivably result in the observed anemia of the dosed animals (Table 3). The platelet count recovered within the two-week post-treatment observation period in the lower dosing groups (1, 3 or 10 mg/kg), but not the 50 mg/kg dosing group (Figure 15). The reversibility of thrombocytopenia observed in the 1, 3 and 10 mg/kg dosing

groups and increased reticulocyte count (days 7 and 14 in the 10 and 50 mg/kg dosing groups) suggest that the platelet production by the bone-marrow was unimpaired by the antibody treatment. The symptoms observed in Y-443-treated Cynos were similar to symptoms of thrombocytopenia (bleeding tendency, hemorrhage in organs, and splenomegaly), which were likely to be target mediated toxicity. ITP is occasionally caused by auto-antibodies against self-antigens on platelets (McMillan et al., 1987; Semple et al., 1995; Coopamah et al., 2003). Consequently, the presented data suggests that Y-443 might act like an autoantibody in Cynos by inducing ITP-like symptoms presumably causing phagocytosis of Y-443-bound platelets by macrophages in the spleen.

Previous reports suggested that disruption of the interaction of autoantibodies and FcγRI is useful in preventing phagocytosis of the antibody-coated platelets by macrophages (Bussel et al., 2000). Additionally, multiple studies utilizing Fc engineering demonstrated that the mutations of Leu235 were capable of diminishing the Fc-FcγRI interaction (Duncan et al., 1988; Jefferis et al., 1990; Chappel et al., 1991; Lund et al., 1991; Morgan et al., 1995; Desjarlais et al., 2007). I have shown that ADCC was the main mechanism of tumor regression of anti-Nectin-2 mAb, Y-443, for which binding of the Fc to FcγRIIIa is essential to maintain ADCC. Therefore, I applied Fc engineering to reduce the binding affinity of the Y-443 Fc to FcγRI while maintaining its binding to FcγRIIIa. Mutation of Leu235 resulted in the L235D mutant, Y-443 (L235D), which showed markedly decreased binding to human FcγRI with only a mild reduction (4.5-times) in binding to human FcγRIIIa, as compared to the parental Y-443 antibody. However, as predicted, Y-443 (L235D) showed a 10-fold weaker ADCC against MDA-MB-231 breast cancer cells (Figure 17). Nevertheless, it has been reported that the lack of L-fucose on N-linked oligosaccharide on Asn297 of human IgG_1 antibodies can

enhance their binding affinity to FcγRIIIa and consequently the ADCC. Therefore, I sought to recover the ADCC of Y-443 (L235D) mutant through defucosylation of the N-glycan on the Asn297 using the POTELLIGENT® technology (see Materials and methods) (Shields et al., 2002; Warncke et al., 2012). The defucosylated Y-443 (L235D) variant, Y-634, showed potent ADCC, comparable to that of the Y-443 antibody while further maintaining the diminished binding affinity to human FcγRI as observed with the Y-443 (L235D) mutant (Figure 17 and Table 3). Thus, Y-634 demonstrated diminished thrombocytopenia in the Cynos both upon single and repeated dose administration, but also maintained the anti-tumor effect against breast and ovarian cancer cells in mouse xenograft models (Figure 18, Figure 19 and Table 6). Although I haven't evaluated the binding activities of Y-443 mutants to Cyno FcγRs, it has been reported that human IgG_1 bound to Cyno FcγRI and FcγRIIIa with similar binding affinities to human FcγRI and FcγRIII, respectively (Roders et al., 2006). In addition, the amino acid sequence of the human IgG_1 binding sites on Cyno FcγRI and FcγRIIIa are nearly identical to those in human FcγRI and FcγRIIIa, respectively (Kanda et al., 2006; Kiyoshi et al., 2015). Therefore, the improved features in Y-634 presumably reflect the binding activities to Cyno FcγRI and FcγRIIIa.

In summary, I demonstrated a potential strategy to overcome ITP-like toxicity of therapeutic antibodies by combining a single amino acid mutation in Fc region and glyco-engineering. These findings may help facilitate the development of antibody therapeutics through a strategy to reduce observed side effects like thrombocytopenia while maintaining antibody efficacy.

Tables and Figures

Table 3. Hematology of Y-443-treated Cynos.

Tested article	Animal number	Day	Erythrocytes ($\times 10^4/\mu L$)	Hematocrit (%)	Hemoglobin (g/dL)	Platelets ($\times 10^4/\mu L$)	Reticulocytes ($\times 10^4/\mu L$)
Control	1M001 (male)	-4	653	41.3	13.1	45.2	2.6
		1	601	38.0	12.0	39.8	3.0
		7	599	38.4	12.1	40.4	5.4
		14	584	37.6	11.7	36.2	4.7
	1M002 (male)	-4	636	40.5	11.7	47.5	1.9
		1	613	38.7	11.3	54.2	1.8
		7	638	40.1	12.2	56.5	4.5
		14	602	37.5	11.4	61.3	4.2
	1F001 (female)	-4	587	40.8	12.3	64.0	2.3
		1	522	36.3	11.0	61.4	2.1
		7	534	37.5	11.4	69.7	8.5
		14	541	38.2	11.6	60.9	7.0
	1F002 (female)	-4	480	37.7	12.2	37.7	6.2
		1	476	37.1	12.2	36.1	5.2
		7	489	38.0	12.7	38.0	6.4
		14	492	37.8	12.7	39.6	6.4
Y-443 10 mg/kg	2M001 (male)	-4	563	38.3	12.2	40.3	10.1
		1	533	36.2	11.2	3.0	11.2
		7	514	34.0	11.2	5.6	23.1
		14	548	36.5	11.4	36.3	16.4
	2M002 (male)	-4	587	42.2	14.0	44.1	8.8
		1	553	38.9	13.3	19.4	8.8
		7	527	36.1	12.2	7.4	28.5
		14	549	36.3	12.6	9.0	30.2
	2F001 (female)	-4	637	41.2	13.1	40.4	1.9
		1	581	37.2	11.5	5.5	7.0
		7	566	34.5	11.3	6.5	18.7
		14	569	35.3	11.4	40.2	15.4
	2F002	-4	474	38.3	12.5	49.5	5.7

	(female)	1	478	39.0	12.5	38.7	11.0
		7	475	38.4	12.7	20.9	17.1
		14	482	38.8	12.7	45.0	15.4
Y-443	3M001	-4	663	41.6	13.4	33.5	4.0
	(male)	1	648	39.8	12.9	1.4	5.2
50		7	599	36.1	12.2	2.4	18.6
mg/kg		14	633	38.4	12.5	4.1	13.9
	3M002	-4	619	40.9	12.7	35.0	2.5
	(male)	1	603	39.5	12.1	0.7	3.0
		7	496	32.2	10.0	1.1	15.4
		14	487	32.7	9.9	4.8	24.4
	3F001	-4	570	38.5	12.2	37.3	5.7
	(female)	1	547	36.8	11.6	1.3	5.5
		7	424	29.5	9.3	3.7	57.7
		14	535	37.5	11.5	9.7	14.4
	3F002	-4	683	41.3	11.7	53.9	4.1
	(female)	1	655	38.4	11.0	1.3	6.6
		7	423	23.7	7.2	2.0	36.4
		14	440	27.4	7.7	5.6	41.8

Table 4. Bleeding time, coagulation factors and spleen weight of Y-443-treated Cynos at 2 weeks after dosing.

Tested article	Dose (mg/kg)	Sex	Animal number	Bleeding time day 15 (min)	Coagulation test (day 14)			Spleen weight (% of body weight)
					PT (s)	APTT (s)	Fibrinogen (mg/dl)	
Control	0	Male	1M001	1.5	9.3	19.1	231	0.17
			1M002	3.5	8.7	18.8	214	0.23
		Female	1F001	1.5	8.7	18.8	239	0.1
			1F002	1.5	9.3	25.9	151	0.06
Y-443	10	Male	2M001	2.5	9.3	20.1	221	0.28
			2M002	5	9.8	19.3	196	0.29
		Female	2F001	1.5	9.4	18.5	253	0.18
			2F002	2	8.2	18	174	0.12
Y-443	50	Male	3M001	6	9.9	20.1	157	0.32
			3M002	17	9.3	19.2	187	0.35
		Female	3F001	3	9	18.5	228	0.25
			3F002	12.5	9.2	17.9	200	0.24

Table 5. Binding activity of Y-443 and Fc-mutated antibodies to human Nectin-2 and human FcγRs.

	K_D values against human Nectin-2	*Relative binding activity to human FcγRs (%)			
		FcγRI	FcγRIIa	FcγRIIb	FcγRIIIa (158F)
Y-443	3.2 nM	100	100	100	100
Y-443 (L235Y)	3.3 nM	0.017	26	35	3.4
Y-443 (L235D)	1.5 nM	0.074	64	120	22
Y-634	3.2 nM	0.056	46	81	300

*Relative binding activity (%) = EC50 (Y-443) / EC50 (sample) x 100

Table 6. Hematology of Y-634-treated Cynos.

Tested article	Animal number	Day	Erythrocytes ($\times 10^4/\mu L$)	Hematocrit (%)	Hemoglobin (g/dL)	Platelets ($\times 10^4/\mu L$)	Reticulocytes ($\times 10^4/\mu L$)
Y-634	1F001	-4	608	39.2	10.9	61.4	2.4
	(female)	1	620	39.5	11.1	40.8	1.2
10		3	578	37.3	10.3	35.5	1.7
mg/kg		7	581	37.8	10.5	42.6	4.6
		10	577	37.3	10.4	38.9	4.0
		14	573	37.4	10.4	48.2	4.0
		17	575	37.7	10.4	48.8	2.9
	1F002	-4	574	39.1	11.3	39.0	4
	(female)	1	548	37.3	11.1	29.8	3.8
		3	532	36.1	10.5	29.5	4.8
		7	555	37.7	11.1	36.3	6.1
		10	554	37.4	11.0	26.0	2.2
		14	549	37.6	11.0	33.7	3.8
		17	527	36.1	10.6	36.6	4.7

Figure 14. Anti-tumor effect of Y-443 in a mouse subcutaneous xenograft model with MDA-MB-231 breast cancer cells.

MDA-MB-231 breast cancer cells were subcutaneously inoculated with Matrigel into a flank of C.B17/Icr-scid/scid mice. On days 34, 41 and 48 after the cell inoculation, Y-443 at a dose of 0.1, 0.3, 1, 3, 10 mg/kg or vehicle was intravenously administered (n = 5). The results are the mean ± S.D. of tumor volume. **: $p < 0.001$ versus the tumor volume treated with vehicle by one-tailed Williams' test.

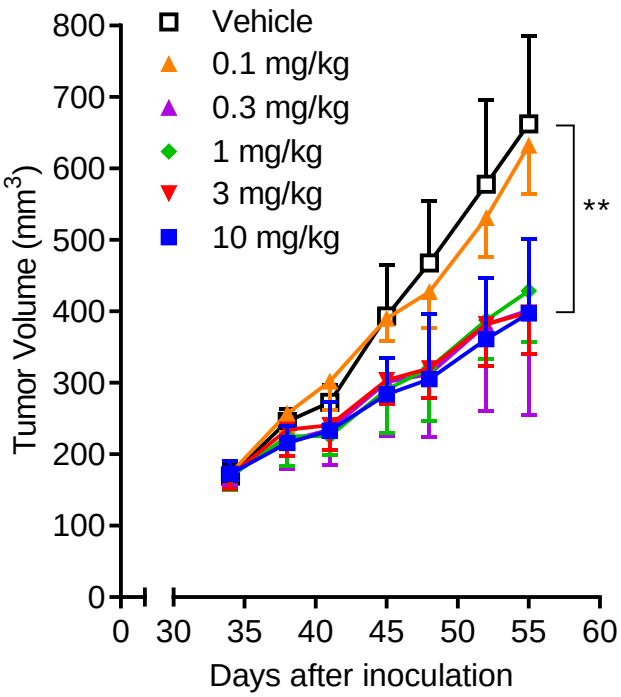
Vehicle
0.1 mg/kg
0.3 mg/kg
1 mg/kg
3 mg/kg
10 mg/kg
Tumor Volume (mm3)
800
700
600
500
400
300
200
100
0
0
30
35
40
45
50
55
60
Days after inoculation
**

Figure 15. Thrombocytopenia induced by single intravenous administration of Y-443 in Cynos.

Platelet count was measured at predose (expressed as day 0) and on days 1, 4, 7 and 14 after the injection of vehicle or Y-443 (1 mg/kg, 3 mg/kg, 10 mg/kg or 50 mg/kg). Each line indicates platelets count of individual monkey. Closed circle and closed square are the result of males, and open circle and open square are the ones of females.

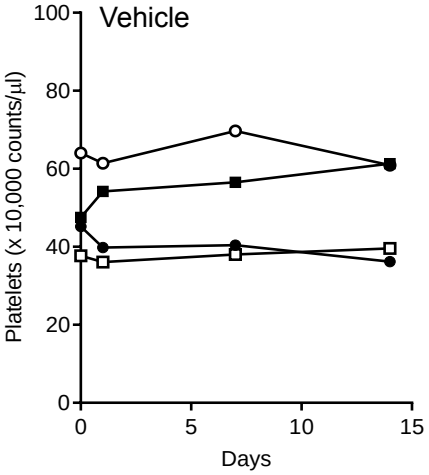
Vehicle
Platelets (x 10,000 counts/µl)
Days
0
20
40
60
80
100
0
5
10
15

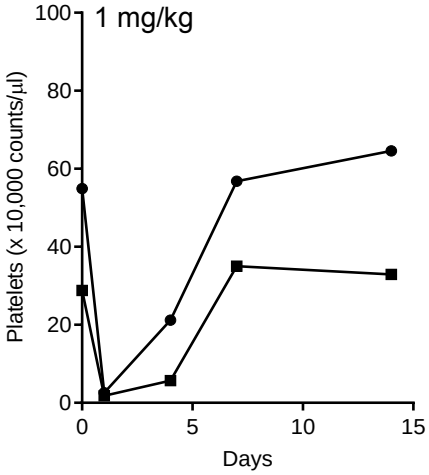
1 mg/kg
Platelets (x 10,000 counts/µl)
Days
0
20
40
60
80
100
0
5
10
15

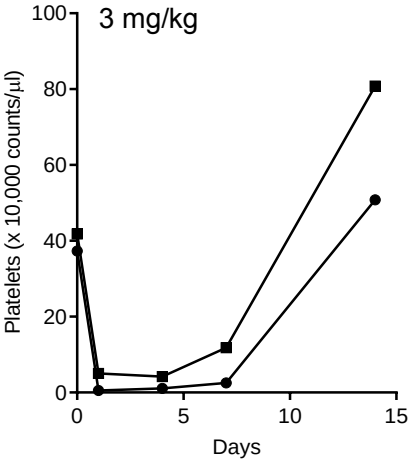
3 mg/kg
Platelets (x 10,000 counts/µl)
Days
0
20
40
60
80
100
0
5
10
15

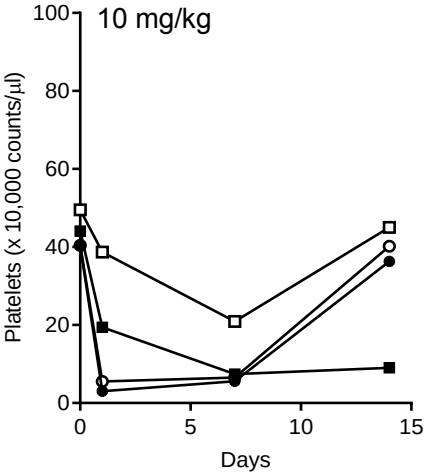
10 mg/kg
Platelets (x 10,000 counts/µl)
Days
0
20
40
60
80
100
0
5
10
15

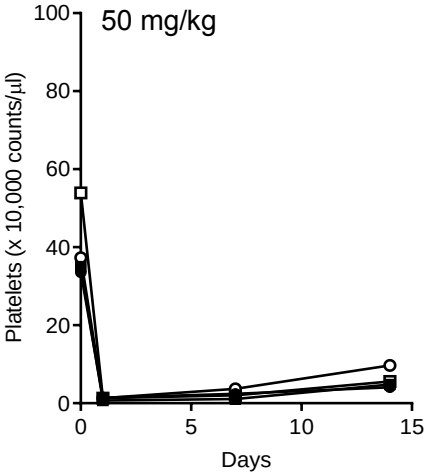
50 mg/kg
Platelets (x 10,000 counts/µl)
Days
0
20
40
60
80
100
0
5
10
15

Figure 16. Serum concentration of Y-443 after a single intravenous administration to Cynos.

Cyno sera were corrected 0, 1, 4, 8, 24, 168, 264 and 336 hours after a bolus injection of Y-443 at 1 mg/kg and 3 mg/kg (n = 2), or 0, 1, 4, 8, 24, 168 and 336 hours after the injection of Y-443 at 10 mg/kg and 50 mg/kg (n = 4). Y-443 concentrations in the Cyno sera were measured by ELISA. The results are the mean ± S.D. of serum antibody concentration. *: lower concentration than the quantification limit (5 ng/mL).

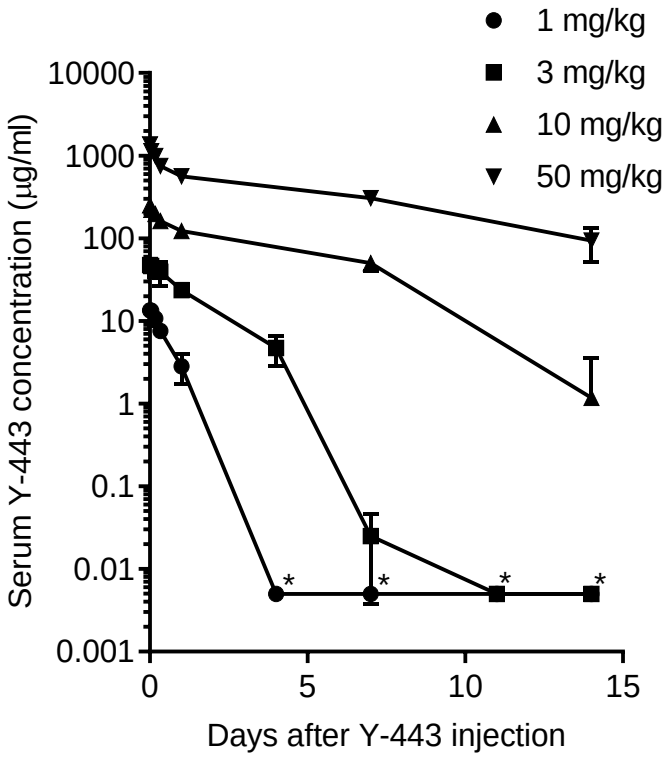
1 mg/kg
3 mg/kg
10 mg/kg
50 mg/kg
Serum Y-443 concentration (μg/ml)
10000
1000
100
10
1
0.1
0.01
0.001
0
5
10
15
Days after Y-443 injection
*
*
*
*

Figure 17. ADCC of Y-443 and Fc-mutated antibodies against MDA-MB-231 cells. MDA-MB-231 cells pre-labeled with Calcein AM were incubated with different concentrations of Y-443 or the Fc mutants, followed by addition of PBMC effector cells at a ratio of 1:50. The cell mixture was incubated for 4 hours at 37°C, and Calcein AM intensity in cells was detected by Acumen eX3 (TTP labtech). The results are the mean ± S.D. of dead cell ratio.

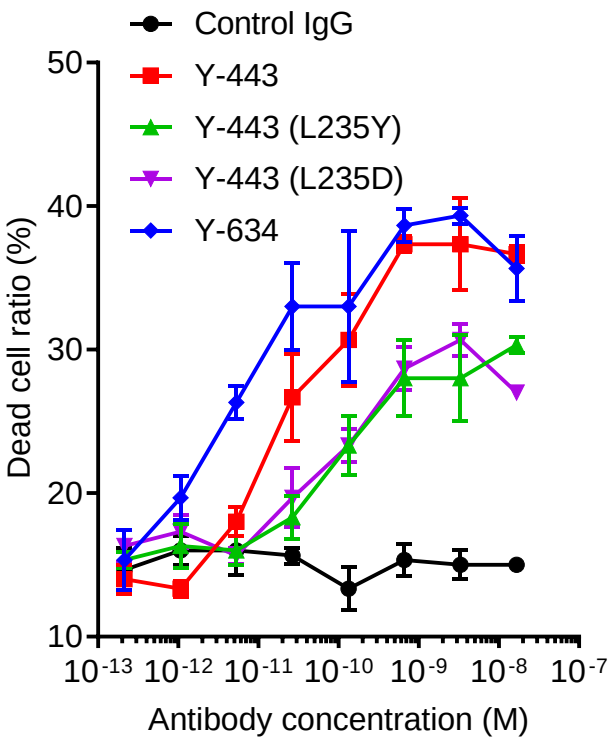
Control IgG
Y-443
Y-443 (L235Y)
Y-443 (L235D)
Y-634
Dead cell ratio (%)
50
40
30
20
10
10-13 10-12 10-11 10-10 10-9 10-8 10-7
Antibody concentration (M)

Figure 18. Thrombocytopenia induced by single and repeated intravenous administration of Y-634 in Cynos.

For the single dose group (A), platelet count was measured in Cynos treated with 10 mg/kg of Y-634 at predose (expressed as day 0) and on days 1, 3, 7, 10, 14 and 17. For the weekly repeated intravenous administration (B) of 3 mg/kg (red lines) or 10 mg/kg (blue lines) of Y-634 dosed on days 0, 7 and 14, platelet count was measured in Cynos at predose (expressed as day 0) and on days 1, 3, 7 (pre 2nd dose), 8, 10, 15, 17, 21 and 28. Each line indicates platelet count of individual monkey.

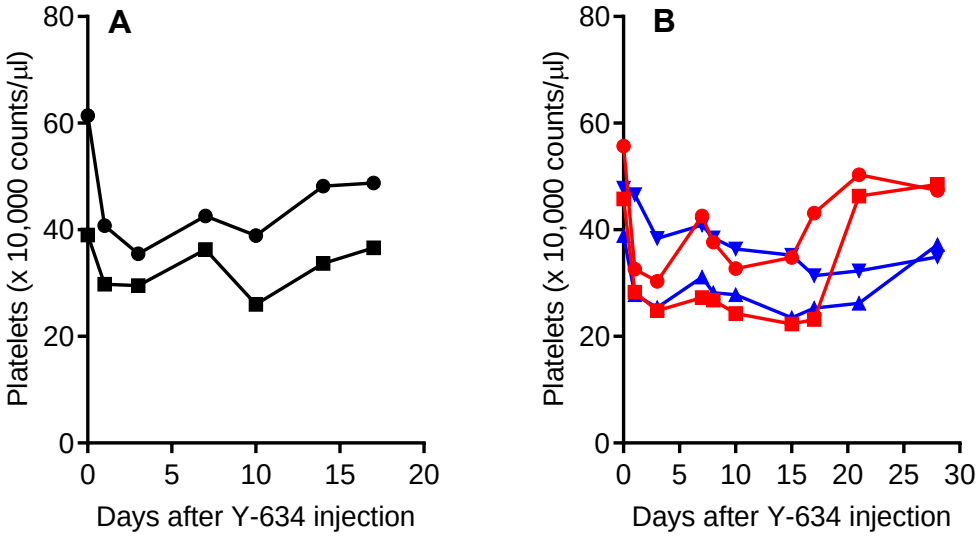
A
B
Platelets (x 10,000 counts/μl)
Days after Y-634 injection
0
20
40
60
80
0
5
10
15
20
25
30

Figure 19. *In vivo* anti-tumor effect of Y-634 in a mouse subcutaneous xenograft model with MDA-MB-231 cells.

Anti-tumor effect of Y-634 was compared with its parental antibody, Y-443, in an MDA-MB-231 mouse subcutaneous xenograft model. On days 37, 44 and 51 after MDA-MB-231 cell inoculation, Y-443 at a dose of 0.3 mg/kg, Y-634 at a dose of 0.1, 0.3 and 1 mg/kg or vehicle was intravenously administered (n = 5). The results are the mean ± S.D. of tumor volume. **: $p < 0.001$ versus the tumor volume treated with vehicle by one-tailed Williams' test.

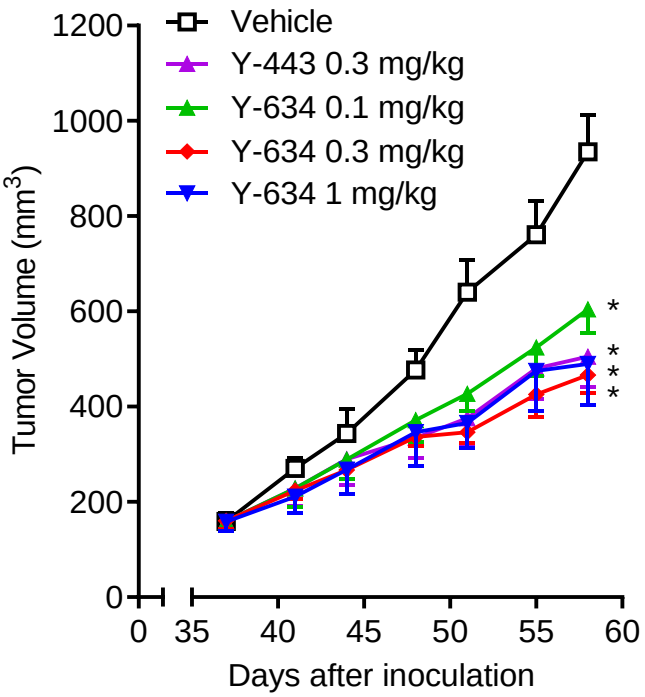
Vehicle
Y-443 0.3 mg/kg
Y-634 0.1 mg/kg
Y-634 0.3 mg/kg
Y-634 1 mg/kg
Tumor Volume (mm3)
1200
1000
800
600
400
200
0
0
35
40
45
50
55
60
Days after inoculation
*
*
*
*

General Discussion

It has been well recognized that the strong potency and low side-effects in cancer by antibody therapeutics are highly valuable for cancer patients compared with traditional chemotherapies, which cause severe side-effects in especially skin, hair, bone marrows since those chemotherapies affect not only cancer cells, but also rapid growth normal cells as well.

Through my studies, I focused on novel cancer target for antibody therapeutic to discover new therapeutic agent, which is safer, more potent, and for treatment of wider cancer patient population. I discovered the overexpression of Nectin-2 gene and protein in multiple cancer tissues, and generated Nectin-2 specific fully human monoclonal antibodies. These antibodies had epitope bin dependent multiple *in vitro* biological functions and superior anti-tumor potencies in *in vivo* studies with ADCC as one of the mechanisms of action. It is not surprising since the clinically validated antibody therapeutics, rituximab (anti-CD20 antibody) and trastuzumab (anti-Her2 antibody), have also been suggested ADCC as a main mechanism for anti-cancer effect (Clynes et al., 2000). Since Nectin-2 *trans*-binding inhibition and *in vitro* cancer cell growth inhibition were not required for *in vivo* anti-tumor effect through the study using Y-167 IgG_4, I have selected Y-443 antibody, epitope bin VII with high ADCC and no other biological functions, as a candidate to eligible unnecessary adverse effects. It is said that ADCC favors a membrane proximal epitope (Cleary et al., 2017). I have not detected epitope of each antibody, however, Y-443 most likely binds to a membrane proximal epitope in Nectin-2. Y-443 has shown cross-reactivity to Cyno Nectin-2 with similar binding affinity. I have never performed the *in vitro* functional studies using anti-human Nectin-2 antibodies against Cyno Nectin-2. However, since the homology of Nectin-2 between human and Cyno is 95% identical, and the binding of Y-443 to

Cyno Nectin-2 is very similar to human Nectin-2, Y-443 most likely induces ADCC in Cyno as well. Y-443 induced thrombocytopenia-like side effect in Cyno, however, the Fc modified antibody, Y-634, diminished the side effect with strong anti-tumor activity. This finding proved that my hypothesis which the side effect induced by Y-443 was triggered by the binding of antibody and FcγRI on macrophages resulting in platelet reduction.

E-cadherin, which is a transmembrane glycoprotein playing a key role in the connection of epithelial cells at adherens junctions. In normal cells, this molecule exerts its tumor suppressing role by activating proliferative Wnt signaling pathway. Despite normal cell functions, E-cadherin downregulation has been reported in multiple cancers such as gastric cancer, colon cancer and breast cancer (Jie et al., 2013; Xing et al., 2013; Horne et al., 2014). The reduction of E-cadherin expression results in the activation of cell proliferation by loss of adhesion efficacy, loss of Wnt signaling activation, and loss of other intracellular signaling (Wong et al., 2018). In normal cells, cell proliferation is inhibited by cell density, often attributed to cell-cell contact. Contact inhibition of proliferation is important for development of normal differentiated tissues and is tightly regulated for proper tissue morphogenesis and organ development. Once normal cells grow to high density, they stop proliferation, however, when normal cells reduce E-cadherin expression (cell adhesion), they continue proliferating on top of each other and lose contact inhibition of cell proliferation. Therefore, the loss of cell adhesion molecule induces uncontrolled cell proliferation. Nectin-2 is also one of cell-adhesion molecule. However, I discovered that Nectin-2 is upregulated in multiple cancer tissues and cancer cell lines. The hypothesis of this upregulation is that Nectin-2 acts as an immune checkpoint molecule, which is crucial for self-tolerance preventing the immune system

by attacking immune cells, like T cells and NK cells. Nectin-2 *cis*-dimer *trans*-binds to Nectin-3 and Nectin-2 expressed on other cells, but also binds to TIGIT and DNAM1. TIGIT is a newly discovered immune checkpoint protein expressed on T cells and NK cells. TIGIT contains an Ig-like domain and an ITIM domain in its cytoplasmic domain, therefore, TIGIT is thought as an inhibitory receptor, which modulates the immune activity by competing with activating receptor, DNAM-1. Anti-TIGIT agonist antibody decrease the expression of T-bet, GATA3, IRF4 and RORc for Th1, Th2, Th9, and Th17 cells with inhibition of IFN-γ production (Lozano et al., 2012). Knockdown of TIGIT in mouse results in increased T-bet and IFN-γ with decreased IL-10, and these effects can be overcome by blocking DNAM-1 signaling, suggesting that TIGIT can inhibit T cell functions by competing with DNAM-1. This TIGIT/DNAM-1 signaling is similar to CTLA4/CD28 pathway, which has been intensively investigated as immune checkpoint inhibitor and activator in human T cell, especially for cancer treatment. Since TIGIT exerts immunosuppressive effects by competing with DNAM-1, Nectin-2 expressed on cancer cells may induce immunosuppressive effects through TIGIT on T cells and NK cells to escape from immune systems. Furthermore, Guillerey et al. demonstrated that multiple myeloma progression was associated with high levels of TIGIT expression on $CD8^+$ T cells (Guillerey et al., 2018). In their report, TIGIT-deficient mice showed reduced tumor burden and prolonged survival, indicating that TIGIT limits antimyeloma immune responses. Also, the blockade of TIGIT function by monoclonal antibody resulted in prolongation of survival in multiple myeloma mouse model. This anti-multiple myeloma potency was significant compared with anti-PD-1 monoclonal antibody. PD-1/PD-L1 is another well-investigated immune checkpoint proteins. PD-1 is also immunosuppressive molecule, like CTLA4 and TIGIT, expressed on T cells and

NK cells. Nivolumumab, marketed as Opdivo, is a human IgG_4 antibody therapeutic, which binds to the PD-1 and blocks its interaction with PD-L1 and PD-L2 resulting in the inhibition of immune suppressive signal through PD-1 in T cells and induction of tumor growth suppression (Angelousi et al., 2018). It is clinically proven that the immune checkpoint inhibitor treating cancer patients induces crucial potency in inhibition of cancer growth by activating T cell function through the blockade of immune suppressive molecules. Astonishingly, antibody co-blockade of TIGIT and PD-L1 by each monoclonal antibody synergistically and specifically enhances $CD8^+$ T cell effector function, resulting in significant tumor and viral clearance (Johnston et al., 2014). In addition to the report, Grapin et al. also demonstrated that combination therapy of anti-TIGIT antibody and anti-PD-L1 antibody in fractionated radiotherapy induced additive/synergistic anti-tumor effects (Grapin et al., 2019). Based on those published findings about TIGIT as an immune suppressive protein and my finding about over-expression of Nectin-2 in cancer cells, there are two or more potential novel therapies for cancer treatment against Nectin-2. First is bispecific antibody against Nectin-2 and PD-L1 on cancer cells to deactivate immune suppressive proteins such as TIGIT and PD-1 (Figure 20). Bispecific antibody contains two unique heavy chains and light chains, which can bind two distinct epitopes of same or different targets. In oncology, only two bispecific antibodies have been approved for use in the clinic, one is Catumaxomab, targeting epithelial cell adhesion molecule and CD3, another is Blinatumomab, targeting CD19 and CD3 (Suurs et al., 2019). Nivolumab is not approved for the use in breast cancer and ovarian cancer, and TIGIT expression in these cancers has been unclear yet. However, since the combination of TIGIT and PD-L1 antibodies demonstrated significant anti-tumor effects, bispecific antibody against

Nectin-2 and PD-L1 has potential to induce strong reduction of immune suppressive effect by blocking TIGIT and PD-1 on T cell, which results in the activation of T cell to kill cancer cells. TIGIT, immune suppressive protein, and DNAM-1, immune activation protein, bind to Ig1 domain in Nectin-2 (Liu et al., 2012; Deuss et al., 2017). Therefore, it is unclear whether it is possible to discover anti-Nectin-2 monoclonal antibodies, which inhibit Nectin-2-TIGIT binding, but do not inhibit Nectin-2-DNAM-1. These antibodies have potential to inhibit TIGIT immune suppressive function and remain DNAM-1 immune activate function. If the antibody discovery is succeeded, the bispecific antibody is relatively easy to generate by molecular biology method. Thus obtained bispecific antibody should be applied Leu235 mutation and defucosylation to minimize the thrombocytopenia-like side effect and to enhance ADCC to suppress cancer cell growth. This bispecific antibody may have superior anti-tumor effect through self-immune mechanisms and ADCC. The second potential therapy against Nectin-2 is to use BiTE (bispecific T cell engagers) technology. BiTEs are fusion proteins consisting of two single chain variable fragments (scFvs) of different antibodies. One of the scFvs binds to T cells via CD3 receptor, and the other scFv binds to a tumor cell via a tumor specific molecule (Baeuerle et al., 2009). By using this technology with targeting Nectin-2 and CD3, it is possible to block immune suppressing effect through TIGIT by Nectin-2 and to engage cytotoxic T cells expressing CD3 on surface and cancer cell expressing Nectin-2 resulting in cancer cell killing. Other alternative target will be Nectin-2 on cancer cell and PD-L1 on $CD8^+$ T cell. This approach will enable to kill cancer cells by blocking both Nectin-2/TIGIT and PD-1/PD-L1 immunosuppressive effects and by connecting cancer cells and cytotoxic T

cells. Since BiTE technology does not have Fc region, the thrombocytopenia-like side effect will be ignored.

In conclusion, my first study suggests Nectin-2 as a potential cancer specific target for antibody therapeutics. In addition, my second study provides a potential strategy to overcome ITP-like toxicity of therapeutic antibodies by combining a single amino acid mutation in Fc region and glycol-engineering. It is highly valuable that my studies shed the light on a novel antibody therapeutics possibly through the inhibition of immune checkpoint and the development of antibody therapeutics through a strategy to reduce observed side effects like thrombocytopenia while maintaining antibody efficacy.

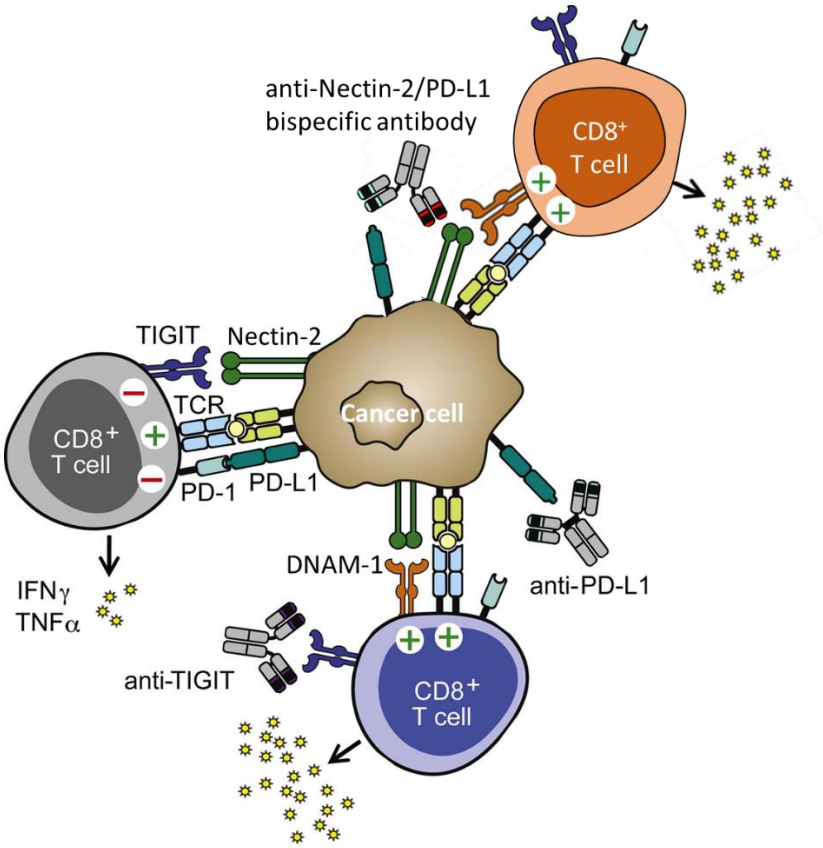

Figure 20. Novel strategies to reactivate exhausted anti-tumor immune responses with antibody blockade of T cell coinhibitory receptors, PD-1/PD-L1 and Nectin-2/TIGIT.

Illustration modified from Johnston et al. (2014). Anti-PD-L1 or anti-TIGIT antibody is able to inhibit immune suppressive signal in $CD8^+$ T cell. Combination therapy of anti-PD-L1 and anti-TIGIT antibodies induced significant anti-tumor activities (Johnston et al., 2014). Therefore, bispecific antibody against Nectin-2 and PD-L1 has potential to mimic the combination therapy to induce superior efficacy as a single agent.

Acknowledgements

I would like to express my deep gratitude to Professor Kentaro Nakano, University of Tsukuba, for being in charge of this dissertation, and for his valuable guidance and encouragement.

I am deeply grateful to Professors Tetsuo Hashimoto, Yuji Inagaki, and Kyoichi Sawamura, University of Tsukuba, for their appropriate advice during the preparation of this dissertation and for valuable discussions through my doctoral program.

I also thank Dr. Tomofumi Kurokawa, Taisho Pharmaceutical Company Limited, and Professor Toshio Kokubo, University of Tsukuba, for valuable suggestions, contributions and helpful supports.

I also thank Dr. Antara Banerjee, Takeda California Inc., for understanding and support on my doctoral program.

Finally, I would like to appreciate my family for supporting my life in University of Tsukuba.

References

- Alewine C., Hassan R., and Pastan I. (2015). Advances in anticancer immunotoxin therapy. Oncologist 20, 176-185
- Angelousi A., Chatzellis E., and Kaltsas G. (2018). New molecular, biological, and immunological agents inducing hypotphysitis. Neuroendocrinology 106, 89-100
- Aoki J., Koike S., Asou H., Ise I., Suwa H., Tanaka T., Miyasaka M., and Nomoto A. (1997). Mouse homolog of poliovirus receptor-related gene 2 product, mPRR2, mediates homophilic cell aggregation. Exp Cell Res 235, 374-384
- Baeuerle P. A., and Reinhardt C. (2009). Bispecific T-cell engaging antibodies for cancer therapy. Cancer Res 69, 4941-4944
- Beck A., Goetsch L., Dumontet C., and Corvaïa N. (2017). Strategies and challenges for the next generation of antibody-drug conjugates. Nat Rev Drug Discov 16, 315-337
- Bottino C., Castriconi R., Pende D., Rivera P., Nanni M., Carnemolla B., Cantoni C., Grassi J., Marcenaro S., Reymond N., Vitale M., Moretta L., Lopez M., and Moretta A. (2003). Identification of PVR (CD155) and Nectin-2 (CD112) as cell surface ligands for the human DNAM-1 (CD226) activating molecule. J Exp Med 198, 557-567
- Bouchard M. J., Dong Y., McDermott B. M. Jr., Lam D. H., Brown K. R., Shelanski M., Bellve A. R., and Racaniello V. R. (2000). Defects in nuclear and cytoskeletal morphology and mitochondrial localization in spermatozoa of mice lacking nectin-2, a component of cell-cell adherens junctions. Mol Cell Biol 20, 2865-2873
- Bussel J. B. (2000). Fc receptor blockade and immune thrombocytopenic purpura.

Semin. Hematol 37, 261-266

- Castriconi R., Dondero A., Corrias M. V., Lanino E., Pende D., Moretta L., Bottino C., and Moretta A. (2004). Natural killer cell-mediated killing of freshly isolated neuroblastoma cells: critical role of DNAX accessory molecule-1-poliovirus receptor interaction. Cancer Res 64, 9180-9184
- Chan C. J., Andrews D. M., and Smyth M. J. (2012). Receptors that interact with nectin and nectin-like proteins in the immunosurveillance and immunotherapy of cancer. Curr Opin Immunol 24, 246-251
- Chappel M. S., Isenman D. E., Everett M., Xu Y. Y., Dorrington K. J., and Klein M. H. (1991). Identification of the Fcγ receptor class I binding site in human IgG through the use of recombinant IgG_1/IgG_2 hybrid and point-mutated antibodies. Proc Natl Acad Sci USA 88, 9036-9040
- Ciardiello F., Troiani T., Bianco R., Orditura M., Morgillo F., Martinelli E., Morelli M. P., Cascone T., and Tortora G. (2006) Interaction between the epidermal growth factor receptor (EGFR) and the vascular endothelial growth factor (VEGF) pathways: a rational approach for multi-target anticancer therapy. Ann Oncol 17, 109-114
- Cines D. B., and Blanchette V. S. (2002). Immune thrombocytopenic purpura. New Engl J Med 346, 995-1008
- Cleary K. L. S., Chan H. T. C., James S., Glennie M. J., and Cragg M. S. (2017). Antibody distance from the cell membrane regulates antibody effector mechanisms. J Immunol 198, 3999-4011
- Clynes R. A., Towers T. L., Presta L. G., and Ravetch J. V. (2000). Inhibitory Fc receptors modulate *in vivo* cytotoxicity against tumor targets. Nat Med 6, 443-446

- Coopamah M., Garvey M., Freedman J., and Semple J. (2003). Cellular immune mechanisms in autoimmune thrombocytopenic purpura: An update. Transfus Med Rev 17, 69-80
- Debre M., Griscelli C., Bonnet M. C., Carosella E., Phillippe N., Reinert P., Vilmer E., Kaplan C., Teillaud J. L., and Griscelli C. (1993). Infusion of Fcγ fragments for treatment of children with acute immune thrombocytopenic purpura. The Lancet 342, 945-949
- Delboy M. G., Patterson J. L., Hollander A. M., and Nicola A. V. (2006). Nectin-2-mediated entry of a syncytial strain of herpes simplex virus via pH-independent fusion with the plasma membrane of Chinese hamster ovary cells. Virol J 3, 105
- Desjarlais R. J., Karki B. S., Lazar A. G., Richards O. J., Moore L. G., and Carmichael F. D. (2007). Fc variants with optimized Fc receptor binding properties. WO Patent No. WO2007041635 A2
- Deuss F. A., Gully B. S., Rossjohn J., and Berry R. (2017). Recognition of nectin-2 by the natural killer cell receptor T cell immunoglobulin and ITIM domain (TIGIT). J Biol Chem 292, 11413-11422
- Dowell J., and Minna D. J. (2005). Erlotinib hydrochloride. Nature Reviews Drug Discovery 4, 13-14
- Duncan A. R., Woof J. M., Partridge L. J., Burton D. R., and Winter G. (1988). Localization of the binding site for the human high-affinity Fc receptor on IgG. Nature 332, 563-564
- Everds N., Li N., Bailey K., Fort M., Stevenson R., Jawando R., Salyers K., Narayanan P., Stevens E., He C., Nguyen M. P., Tran S., Doyle N., Poitout-Belissent F., Jolette J., Xu C., and Sprugel K. (2013). Unexpected

thrombocytopenia and anemia in cynomolgus monkeys induced by a therapeutic human monoclonal antibody. Toxicol Pathol 41, 951-969

- Fabre S., Reymond N., Cocchi F., Menotti L., Dubreuil P., Campadelli-Fiume G., and Lopez M. (2002). Prominent role of the Ig-like V domain in *trans*-interactions of nectins. Nectin3 and nectin 4 bind to the predicted C-C'-C"-D beta-strands of the nectin1 V domain. J Biol Chem 277, 27006-27013
- Fan Z., and Mendelsohn J. (1998). Therapeutic application of anti-growth factor receptor antibodies. Curr Opin Oncol 10, 67-73
- Ferrara N. (1995). The role of vascular endothelial growth factor in pathological angiogenesis. Breast Cancer Res Treat 36, 127–137.
- Ferrara N., Hillan J. Kenneth., and Novotny W. (2005). Bevacizumab (Avastin), a humanized anti-VEGF monoclonal antibody for cancer therapy. Biochem Biophys Res Commun 333, 328-335
- Fox S. B., Smith K., Hollyer J., Greenall M., Hastrich D., and Harris A. L. (1994). The epidermal growth factor receptor as a prognostic marker: Results of 370 patients and review of 3009 patients. Breast Cancer Res Treat 29, 41-49
- Fukuhara A., Irie K., Nakanishi H., Takekuni K., Kawakatsu T., Ikeda W., Yamada A., Katata T., Honda T., Sato T., Shimizu K., Ozaki H., Horiuchi H., Kita T., and Takai Y. (2002a). Involvement of nectin in the localization of junctional adhesion molecule at tight junctions. Oncogene 21, 7642-7655
- Fukuhara A., Irie K., Yamada A., Katata T., Honda T., Shimizu K., Nakanishi H., and Takai Y. (2002b). Role of nectin in organization of tight junctions in epithelial cells. Genes Cells 7, 1059-1072
- Fukuhara A., Shimizu K., Kawakatsu T., Fukuhara T., and Takai Y. (2003).

Involvement of nectin-activated Cdc42 small G protein in organization of adherens and tight junctions in Madin-Darby canine kidney cells. J Biol Chem 278, 51885-51893

- Go R. S., Johnston K. L., and Bruden K. C. (2007). The association between platelet autoantibody specificity and response to intravenous immunoglobulin G in the treatment of patients with immune thrombocytopenia. Haematologica 92, 283-284
- Grapin M., Richard C., Limagne E., Boidot R., Morgand V., Bertaut A., Derangere V., Laurent P. A., Thibaudin M., Fumet J. D., Crehange G., Ghiringhelli F., and Mirjolet C. (2019). Optimized fractionated radiotherapy with anti-PD-L1 and anti-TIGIT: a promising new combination. J Immunother Cancer 7:160
- Guillerey C., Harjunpää H., Carrié N., Kassem S., Teo T., Miles K., Krumeich S., Weulersse M., Cuisinier M., Stannard K., Yu Y., Minnie S. A., Hill G. R., Dougall W. C., Avet-Loiseau H., Teng M. W. L., Nakamura K., Martinet L., and Smyth M. J. (2018). TIGIT immune checkpoint blockade restores CD8+ T-cell immunity against multiple myeloma. Blood 132, 1689-1694
- Gül N., and van Egmond M. (2015). Antibody-dependent phagocytosis of tumor cells by macrophages: a potent effector mechanism of monoclonal antibody therapy of cancer. Cancer Res 75, 5008-5013
- Horne H. N., Sherman M. E., Garcia-Closas M., Pharoah P. D., Blows F. M., Yang X. R., Hewitt S. M., Conway C. M., Lissowska J., Brinton L. A., Prokunina-Olsson L., Dawson S. J., Caldas C., Easton D. F., Chanock S. J., and Figueroa J. D. (2014). Breast cancer susceptibility risk associations and heterogeneity by E-cadherin tumor tissue expression. Breast Cancer Res Treat 143, 181-187

- Iamele L., Vacchia L., and Scotti C. (2015). Antibody-drug conjugates: targeted weapons against cancer. Antibody tech J 5, 1-13
- Inagaki M., Irie K., Deguchi-Tawarada M., Ikeda W., Ohtsuka T., Takeuchi M., and Takai Y. (2003). Nectin-dependent localization of ZO-1 at puncta adhaerentia junctions between the mossy fiber terminals and the dendrites of the pyramidal cells in the CA3 area of adult mouse hippocampus. J Comp Neurol 460, 514-524
- Ishida Y., Agata Y., Shibahara K., and Honjo T. (1992). Induced expression of PD-1, a novel member of the immunoglobulin gene superfamily, upon programmed cell death. EMBO J 11, 3887-3895
- Jefferis R., Lund J., and Pound J. (1990). Molecular definition of interaction site on human IgG for Fc receptors (huFc gamma R). Molecular Immunology 27, 1237-1240
- Jie D., Zhongmin Z., Guoqing L., Sheng L., Yi Z., Jing W., and Liang Z. (2013). Positive expression of LSD1 and negative expression of E-cadherin correlate with metastasis and poor prognosis of colon cancer. Dig Dis Sci 58, 1581-1589
- Johnston R. J., Comps-Agrar L., Hackney J., Yu X., Huseni M., Yang Y., Park S., Javinal V., Chiu H., Irving B., Eaton D. L., and Grogan J. L. (2014). The immunoreceptor TIGIT regulates antitumor and antiviral CD8(+) T cell effector function. Cancer Cell 26, 923-937
- Kanda Y., Yomane-Ohnuki N., Sakai N., Yamano K., Nakano R., Inoue M., Misaka H., Iida S., Wakitani M., Yano K., Shitara K., Hosoi S., and Satoh M. (2006). Comparison of cell lines for stable production of fucose-negative antibodies with enhanced ADCC. Biotech Bioeng 94, 680-688
- Kiyoshi M., Caaveiro J. M., Kawai T., Tashiro S., Ide T., Asaoka Y., Hatayama K.,

and Tsumoto K. (2015). Structural basis for binding of human IgG_1 to its high-affinity human receptor FcγRI. Nat Commun 6, 6866

- Kurokawa T., Wuhrer M., Lochnit G., Geyer H., Markl J., and Geyer R. (2002). Hemocyanin from the keyhole limpet Megathura crenulata (KLH) carries a novel type of N-glycans with Gal (b1–6) Man-motifs. Eur J Biochem 269, 5459-5473
- Leach D. R., Krummel M. F., and Allison J. P. (1996). Enhancement of antitumor immunity by CTLA-4 blockade. Science 271, 1734-1736
- Liu J., Qian X., Chen Z., Xu X., Gao F., Zhang S., Zhang R., Qi J., Gao G. F., and Yan J. (2012). Crystal structure of cell adhesion molecule nectin-2/CD112 and its binding to immune receptor DNAM-1/CD226. J Immunol 188, 5511-5520
- Lopez M., Aoubala M., Jordier F., Isnardon D., Gomez S., and Dubreuil P. (1998). The human poliovirus receptor related 2 protein is a new hematopoietic/endothelial homophilic adhesion molecule. Blood 92, 4602-4611
- Lozano E., Dominguez-Villar M., Kuchroo V., and Hafler D. A. (2012). The TIGIT/CD226 axis regulates human T cell function. J Immunol 188, 3869-3875
- Lund J., Winter G., Jones P. T., Pound J. D., Tanaka T., Walker M. R., Artymiuk P. J., Arata Y., Burton D. R., and Jefferis R. (1991). Human FcγRI and FcγRII interact with distinct but overlapping sites on human IgG. J Immunol 147, 2657-2662
- Maron B. S., Alpert L., Kwak A. H., Lomnicki S., Chase L., Xu D., O'Day E., Nagy J. R., Lanman B. R., Cecchi F., Hembrough T., Schrock A., Hart J., Xiao S., Setia N., and Catenacci V. T. D. (2018). Targeted Therapies for Targeted Populations: Anti-EGFR Treatment for EGFR-Amplified Gastroesophageal Adenocarcinoma. Cancer Disc 8, 696-713

- Mattes M. J., (2002). Radionuclide-antibody conjugates for single-cell cytotoxicity. Cancer 94, 1215-1223
- McMillan R., Tani P., Millard F., Berchtold P., Renshaw L., and Woods V. L. Jr. (1987). Platelet-associated and plasma anti-glycoprotein autoantibodies in chronic ITP. Blood 70, 1040-1045
- Miyahara M., Nakanishi H., Takahashi K., Satoh-Horikawa K., Tachibana K., and Takai Y. (2000). Interaction of nectin with afadin is necessary for its clustering at cell-cell contact sites but not for its *cis* dimerization or *trans* interaction. J Biol Chem 275, 613-618
- Mizoguchi A., Nakanishi H., Kimura K., Matsubara K., Ozaki-Kuroda K., Katata T., Honda T., Kiyohara Y., Heo K., Higashi M., Tsutsumi T., Sonoda S., Ide C., and Takai Y. (2002). Nectin: an adhesion molecule involved in formation of synapses. J Cell Biol 156, 555-565
- Momose Y., Honda T., Inagaki M., Shimizu K., Irie K., Nakanishi H., and Takai Y. (2002). Role of the second immunoglobulin-like loop of nectin in cell-cell adhesion. Biochem Biophys Res Commun 293, 45-49
- Morgan A., Jones N. D., Nesbitt A. M., Chaplin L., Bodmer M. W., and Emtage J. S. (1995). The N-terminal end of the CH2 domain of chimeric human IgG_1 anti-HLA-DR is necessary for C1q, FcγRI and FcγRIII binding. Immunology 86, 319-324
- Morita H., Nandadasa S., Yamamoto T. S., Terasaka-Iioka C., Wylie C., and Ueno N. (2010). Nectin-2 and N-cadherin interact through extracellular domains and induce apical accumulation of F-actin in apical constriction of Xenopus neural tube morphogenesis. Development 137, 1315-1325

- Ober R. J., Radu C. G., Ghetie V., and Ward E. S. (2001). Differences in promiscuity for antibody-FcRn interactions across species: implications for therapeutic antibodies. Intl Immunol 13, 1551-1559
- Pende D., Spaggiari G. M., Marcenaro S., Martini S., Rivera P., Capobianco A., Falco M., Lanino E., Pierri I., Zambello R., Bacigalupo A., Mingari M. C., Moretta A., and Moretta L. (2005). Analysis of the receptor-ligand interactions in the natural killer-mediated lysis of freshly isolated myeloid or lymphoblastic leukemias: evidence for the involvement of the Poliovirus receptor (CD155) and Nectin-2 (CD112). Blood 105, 2066-2073
- Reymond N., Fabre S., Lecocq E., Adelaide J., Dubreuil P., and Lopez M. (2001). Nectin4/PRR4, a new afadin-associated member of the nectin family that *trans*-interacts with nectin1/PRR1 through V domain interaction. J Biol Chem 276, 43205-43215
- Rogers K. A., Scinicariello F., and Attanasio R. (2006). IgG Fc receptor III homologues in nonhuman primate species: genetic characterization and ligand interactions. J Immunol 177, 3848-3856
- Satoh-Horikawa K., Nakanishi H., Takahashi K., Miyahara M., Nishimura M., Tachibana K., Mizoguchi A., and Takai Y. (2000). Nectin-3, a new member of immunoglobulin-like cell adhesion molecules that shows homophilic and heterophilic cell-cell adhesion activities. J Biol Chem 275,10291-10299
- Semple J. W., and Freedman J. (1995). Abnormal cellular immune mechanisms associated with autoimmune thrombocytopenia. Transfusion Medicine Reviews 9, 327-338
- Shields R. L., Lai J., Keck R., O'Connell L. Y., Hong K., Meng Y. G., Weikert S.

H., and Presta L. G. (2002). Lack of fucose on human IgG_1 N-linked oligosaccharide improves binding to human Fcgamma RIII and antibody-dependent cellular toxicity. J Biol Chem 277, 26733-26740

- Stanietsky N., Simic H., Arapovic J., Toporik A., Levy O., Novik A., Levine Z., Beiman M., Dassa L., Achdout H., Stem-Ginossar N., Tsukerman P., Jonjic S., and Mandelboim O. (2009). The interaction of TIGIT with PVR and PVRL2 inhibits human NK cell cytotoxicity. Proc Natl Acad Sci U. S. A. 106, 17858-17863
- Steplewski Z., Sun L. K., Shearman C. W., Ghrayeb J., Daddona P., and Koprowski H. (1988). Biological activity of human-mouse IgG_1, IgG_2, IgG_3, and IgG_4 chimeric monoclonal antibodies with antitumor specificity. Proc Natl Acad Sci U. S. A. 85, 4852-4856
- Suurs F. V., Lub-de Hooge M. N., de Vries E. G. E., and de Groot D. J. A. (2019). A review of bispecific antibodies and antibody constructs in oncology and clinical challenges. Pharmacol Ther 201, 103-119
- Tahara-Hanaoka S., Shibuya K., Kai H., Miyamoto A., Morikawa Y., Ohkochi N., Honda S., and Shibuya A. (2006). Tumor rejection by the poliovirus receptor family ligands of the DNAM-1 (CD226) receptor. Blood 107, 1491-1496
- Tahara-Hanaoka S., Shibuya K., Onoda Y., Zhang H., Yamazaki S., Miyamoto A., Honda S., Lanier L. L., and Shibuya A. (2004). Functional characterization of DNAM-1 (CD226) interaction with its ligands PVR (CD155) and nectin-2 (PRR-2/CD112). Int Immunol 16, 533-538
- Takai Y., and Nakanishi H. (2003). Nectin and afadin: novel organizers of intercellular junctions. J Cell Sci 116, 17-27
- Tao M. H., Canfield S. M., and Morrison S. L. (1991). The differential ability of

human IgG_1 and IgG_4 to activate complement is determined by the COOH-terminal sequence of the CH2 domain. J Exp Med 173, 1025-1028

- Tomizuka K., Shinohara T., Yoshida H., Uejima H., Ohguma A., Tanaka S., Sato K., Oshimura M., and Ishida I. (2000). Double trans-chromosomic mice: maintenance of two individual human chromosome fragments containing Ig heavy and kappa loci and expression of fully human antibodies. Proc Natl Acad Sci U. S. A. 97, 722-727
- Yasumi M., Shimizu K., Honda T., Takeuchi M., and Takai Y. (2003). Role of each immunoglobulin-like loop of nectin for its cell-cell adhesion activity. Biochem Biophys Res Commun 302, 61-66
- Waks G. A., and Winer P. E. (2019). Breast cancer treatment. JAMA 321, 288-300
- Wallace P. K., Keler T., Guyre P. M., and Fanger M. W. (1997). FcγRI blockade and modulation for immunotherapy. Cancer Immunol Immunother 45, 137-141
- Wan H. (2016). An overall comparison of small molecules and large biologics in ADME testing. ADMET & DMPK 4, 1-22
- Wang W., Erbe K. A., Hank A. J., Morris S. Z., and Sondel M. P. (2015). NK cell-mediated antibody-dependent cellular cytotoxicity in cancer immunotherapy. Front Immunol 6: 368
- Warncke M., Calzascia T., Coulot M., Balke N., Touil R., Kolbinger F., and Heusser C. (2012). Different adaptations of IgG effector function in human and nonhuman primates and implications for therapeutic antibody treatment. J Immunol 88, 4405-4411
- Warner M. S., Geraghty R. J., Martinez W. M., Montgomery R. I., Whitbeck J. C., Xu R., Eisenberg R. J., Cohen G. H., and Spear P. G. (1998). A cell surface protein

with herpesvirus entry activity (HveB) confers susceptibility to infection by mutants of herpes simplex virus type 1, herpes simplex virus type 2, and pseudorabies virus. Virology 246, 179-189

- Webster M. L., Sayeh E., Crow M., Chen P., Nieswandt B., Freedman J., and Ni H. (2006). Relative efficacy of intravenous immunoglobulin G in ameliorating thrombocytopenia induced by platelet GPIIb/IIIa versus GPIbalpha antibodies. Blood 108, 943-946
- Wong S. H. M., Fang C. M., Chuah L. H., Leong C. O., and Ngai S. C. (2018). E-cadherin: Its dysregulation in carcinogenesis and clinical implications. Crit Rev Oncol Hematol 121, 11-22
- Xing B. X., Tang Y., Yuan G., Wang Y., Wang J., Yang Y., and Chen M. (2013). The prognostic value of E-cadherin in gastric cancer: A meta‐analysis. Int J Cancer 132, 2589-2596